



Sorption and mobilization of iodine in a tropical forest river catchment – A case study in Costa Rica

Master thesis

26.04.2018

Technical University Braunschweig

Faculty of Architecture, Civil Engineering and Environmental Sciences

Institute of Geoecology

Author:

Laura Piechulla

Matriculation no.: 4663926

l.piechulla@tu-braunschweig.de

Supervisors:

Prof. Dr. Harald Biester

Prof. Dr. Boris Schröder-Esselbach

Date:

26.04.2018

Declaration

I declare that I have authored this thesis independently, that I have not used other than the declared sources, and that I have explicitly marked all material which has been quoted either literally or by content from the used sources.

Eigenständigkeitserklärung

Hiermit versichere ich, die vorliegende Masterarbeit eigenständig und nur unter Verwendung der im Literaturverzeichnis aufgeführten Quellen angefertigt zu haben. Jegliches Material, das direkt oder indirekt zitiert wurde, habe ich explizit gekennzeichnet.

Declared by: Laura Piechulla, born on 27.08.1991 in Hannover, Germany

Braunschweig,

Signature:

Table of contents

List of Tables.....	VI
List of Figures.....	VII
List of Abbreviations.....	X
Assignment.....	1
Abstract.....	2
Zusammenfassung.....	3
1 Introduction.....	4
1.1 Sorption of iodine in soils.....	5
1.1.1 Mechanisms of Iodination.....	6
1.1.2 Sorption to inorganic components.....	7
1.2 Forested mountain watersheds in the tropics.....	9
2 Materials and Methods.....	12
2.1 Study site.....	12
2.2 Study and sampling design.....	13
2.2.1 Sampling of soil.....	13
2.2.2 Sampling of stream water.....	14
2.2.3 Sampling of stream biofilms.....	14
2.2.4 High-resolution stream and climate data.....	14
2.2.5 Sampling of canopy throughfall.....	15
2.3 Chemical analysis.....	15
2.3.1 Soil analysis-sequential extraction of iodine.....	15
2.3.2 Water analysis.....	17
2.3.3 Solid analysis.....	18
2.4 Calculation.....	18
2.4.1 Load and flux calculation.....	18
2.4.2 Classification of precipitation.....	19
2.4.3 Streamflow separation.....	19
2.4.4 Enrichment factor.....	20
2.5 Statistical analysis.....	20
3 Results.....	21
3.1 Sequential extraction.....	21
3.2 Catchment hydrological data.....	25

3.2.1	Frequency distribution of rainfall intensity.....	25
3.2.2	Streamflow discharge.....	27
3.2.3	Separation of baseflow and quickflow.....	27
3.2.4	Stream water chemistry during baseflow and quickflow	28
3.3	Comparison of the streams: Q_M , Q_L and Q_R	32
3.3.1	Physical parameter.....	32
3.3.2	Stream water chemistry of Q_M , Q_L , and Q_R	33
3.3.3	Element fluxes of Q_M , Q_L , and Q_R	35
3.4	Element content in biofilm samples	36
3.5	Parent rock analysis	36
3.6	Iodine enrichment compared to bromine	37
4	Discussion.....	39
4.1	Iodine enrichment and sorption in soils	39
4.1.1	Solid phase iodine binding	40
4.1.2	Water soluble iodine in soils	41
4.1.3	Soil physio-chemical processes: Iodine transport through the soil profile.....	42
4.1.4	Tropical processes affecting iodine geochemistry	44
4.2	Influence of catchment hydrology on iodine discharge.....	45
4.2.1	Contributions of quickflow and baseflow to water chemistry.....	46
4.2.2	Separation of streamflow into baseflow and quickflow based on physical parameters.....	47
4.2.3	Chemical separation of the streamflow.....	47
4.3	Transport of iodine from soils to stream	50
4.3.1	Iodine speciation in Q_M	51
4.3.2	Fate of iodine in stream	52
4.4	Comparison between C_L and C_R	52
4.5	Iodine chemistry compared to Br chemistry based on the I:Br-ratio	54
5	Outlook.....	56
6	Conclusions	56
7	Acknowledgments.....	57
8	References.....	58
9	Appendix	67

List of Tables

Table 1 Classification of rainfall events based on daily intensity	19
Table 2 Spearman correlation coefficients of I in mg kg ⁻¹ [I] and I in percent [%] of the extraction procedures with depth, soil texture and other element concentrations measured by Schulz (2018). Non-significant correlations are marked in grey.....	24
Table 3 Time of peak rain intensity or discharge sorted by water type. P: precipitation; Q _M : total discharge; BQ: baseflow; DQ: quickflow: Here the automatic measurements are depicted	27
Table 4 Mean concentrations (Ca, Mg, K, Na, Cl; DOC, I, Br, Fe) of chemical constituents, discharge (Q), pH and conductivity (EC), redox potential (Eh) sorted by water type. P: precipitation; Q: total stream water in Q _M (all samples); BQ: stream water during baseflow; DQ: stream water during quickflow.....	30
Table 5 Spearman correlation coefficients of the total discharge of Q _M (Q), baseflow (BQ), quickflow (DQ), turbidity, pH, rain and element concentrations. Non-significant correlations are marked in grey	31
Table 6 Concentrations of chemical constituents, sorted by parent rock type. Andesite (A) and volcanic conglomerate (Vc)	36
Table 7 Mean iodine : bromine (I:Br)-ratios in stream water during the entire examination time (Q), baseflow (BQ) and quickflow (DQ) conditions, in leachates, biofilms and parent rocks (Andesite (A) and volcanic conglomerate (Vc))	37
Table 8 Reference materials for solid soil analyses with certified values (CV) and measured values (MV).....	68
Table 9 Reference materials for liquid sample analyses with certified values (CV) and measured values (MV) for stream water (MV).....	69
Table 10 Reference materials for liquid sample analyses with certified values (CV) and measured values (MV) for leachates (F1-F5).....	70

List of Figures

Figure 1 Schematic iodine cycle.	5
Figure 2 Schematic iodine redox cycle.	7
Figure 3 Hydrological pathways. Groundwater and baseflow pathways are shown in grey, stormflow pathways in red (including saturation excess flow), infiltration excess pathways in orange, evapo(transpir)ration in dark yellow.	10
Figure 4 Left: Overview of the San Lorencito catchment, ReBAMB, Costa Rica. Right: Enlarged section (main study area) of the ReBAMB: locations of soil profiles (black points) in the catchments on the right side C_R and the left side C_L ; sampling points for stream water (red pentagons) of the two tributaries (Q_R ; Q_L) and the main stream (Q_M), the research (grey house) and meteorological station (grey triangle). The boundaries of the catchments (ReBAMB, C_R and C_L) are shown in black.....	13
Figure 5 Schematic procedure of each sequential extraction step for iodine fractionation in soil.	15
Figure 6 Schematic diagram of the sequential extraction procedure for iodine fractionation in soil samples.	16
Figure 7 Left: Extractable iodine concentrations [mg kg^{-1}] in percentage of total iodine amounts in the respective soil horizon [%] of each extraction step F1-F5 in profiles L1 (A), L3 (B), R1 (C), R3 (D), R5 (E). Right: Total iodine concentration in soil profiles (measured by Schulz (2018)).	22
Figure 8 Frequency distribution of rainfall intensity based on daily intensities during the time period of sample collection.	25
Figure 9 Hydrograph: 5 min interval precipitation, total discharge with time series of runoff separated into baseflow and quickflow components during A) 05.01-30.06; B) 24.05-16.06 (examination time) and C) during event 1: 27.05 (left) and 2: 28.05 (right). Here the automatic measurements are depicted. Precipitation: blue bars, total discharge: grey line, baseflow: blue line, quickflow: red line.	26
Figure 10 Enrichment factors for all element concentrations during quickflow conditions against baseflow conditions in Q_M . sorted from highest to lowest. Enrichment factor of >1.25 : red bars, enrichment factors between 1.25 and 1: grey bars, depletion factors between	

1 and 0.75: light blue bars, depletion factor of <0.75: dark blue bars. Boundary between enrichment and depletion (enrichment factor of 1): black solid line.	28
Figure 11 Enrichment factors for all element fluxes during quickflow conditions against baseflow conditions sorted from highest to lowest. Enrichment factor of >3: red bars, enrichment factors between 3 and 2: grey bars, enrichment factors between 2 and 1: light blue bars. Boundary between enrichment and depletion (enrichment factor of 1): black solid line.....	29
Figure 12 Boxplots of physical parameters (Q, pH, EC, Eh, Tds) in the main channel Q_M and the two tributaries Q_L and Q_R . Q_M : red bar, Q_L : grey bar, Q_R : blue bar.	32
Figure 13 Enrichment factors for all element concentrations in stream water of Q_R against Q_L sorted from highest to lowest. Enrichment factor of >1.25: red bars, enrichment factors between 1.25 and 1: grey bars, depletion factors between 1 and 0.75: light blue bars, depletion factor of <0.75: dark blue bars. Boundary between enrichment and depletion (enrichment factor of 1): black solid line.	33
Figure 14 Boxplots of element concentrations during sampling period in the main channel Q_M and the two tributaries Q_L and Q_R Manually taken samples only. Q_M : red bar, Q_L : grey bar, Q_R : blue bar.....	34
Figure 15 Enrichment factors for all element fluxes of Q_R against Q_L sorted from highest to lowest. Enrichment factor of >3: red bars, enrichment factors between 3 and 2: grey bars, enrichment factors between 2 and 1: light blue bars, depletion factor of <1: dark blue bars. Boundary between enrichment and depletion (enrichment factor of 1): black solid line.....	35
Figure 16 Concentration of elements in biofilms of Q_M (red), Q_L (grey) and Q_R (blue). I, Br, Y, Zr [mg kg^{-1}] and Fe, Al, Si, S, K, Ca [g kg^{-1}].....	36
Figure 17 Extractable iodine concentrations [mg kg^{-1}] divided by extractable bromine concentrations of F1 in profiles L1 (red), L3 (dark yellow), R1 (black), R3 (grey), R5 (blue). Iodine-bromine-ratios in the respective stream water, biofilm, solid soil samples (measured by Schulz (2018)) and throughfall were shown as black dashed vertical lines.	38
Figure 18 Model of the vertical transport of iodine in soil profiles of the ReBAMB in relationship with organic matter and Fe-oxides.	43

Figure 19 Schematic representation of the hydrologic processes during dry (left side) and during wet conditions (right side) at hillslope scale.....	49
Figure 20 Eh-pH diagram for iodine species in water at 25 °C, adapted from Li et al. (2013). The type of I species expected under thermodynamic considerations in Q_M as the dominant species is shaded red.	52
Figure 21 Schematic representation of the hydrologic processes during wet conditions at hillslope scale in the catchments of the left tributary (C_L) and the right tributary (C_R). The thickness of the arrows symbolises the relative contribution to total discharge in the respective catchment.....	53
Figure 22 Extractable iodine concentrations [mg kg^{-1}] divided by extractable bromine concentration of F2 in profiles L1 (red), L3 (dark yellow), R1 (black), R3 (grey), R5 (blue). Iodine-bromine-ratios in the respective stream water, biofilm, solid soil samples (measured by Schulz (2018)) and throughfall were shown as black dashed vertical lines.	67
Figure 23 Extractable iodine concentrations [mg kg^{-1}] divided by extractable bromine concentration of F3 in profiles L1 (red), L3 (dark yellow), R1 (black), R3 (grey), R5 (blue). Iodine-bromine-ratios in the respective stream water, biofilm, solid soil samples (measured by Schulz (2018)) and throughfall were shown as black dashed vertical lines.	67
Figure 24 Extractable iodine concentrations [mg kg^{-1}] divided by extractable bromine concentration of F4 in profiles L1 (red), L3 (dark yellow), R1 (black), R3 (grey), R5 (blue). Iodine-bromine-ratios in the respective stream water, biofilm, solid soil samples (measured by Schulz (2018)) and throughfall were shown as black dashed vertical lines.	68

List of Abbreviations

BQ	Baseflow
CH₃I	Iodomethane
C_L	Catchment of the left tributary
C_R	Catchment of the right tributary
DOI	Dissolved organic iodine
DOC	Dissolved organic carbon
DOM	Dissolved organic matter
DQ	Quickflow
F1-F5	Step 1-5 of the conducted sequential extraction
EC	Conductivity
Eh	Redox potential
HOI	Hypoiodous acid
HPLC	High performance liquid chromatography
I⁻	Iodide
I₂	Elemental iodine
I₃	Triiodide
IC	Ion chromatography
ICP-MS	Inductively coupled Plasma mass spectrometry
ICP-OES	Inductively coupled Plasma optical emission spectrometry
IDDs	Iodine deficiency disorders
IO₃⁻	Iodate
K_d	Adsorption-desorption distribution coefficient for soils
L1-4	Soil profiles in catchment C _L
OM	Organic matter
Org-I	Organically bound iodine
Q	Discharge, streamflow
Q_L	Tributary on the left side
Q_M	main channel
Q_R	Tributary on the right side
R1-5	Soil profiles in catchment C _R
RDF-method	recursive digital filter technique
ReBAMB	Reserva Biologica Arturo Manuel Brenes
r_s	Spearman correlation coefficient
RT	room temperature
SOM	Soil organic matter
STD	Standard deviation
TdS	Total dissolved solids
XRF	X-ray fluorescence spectrometry

Assignment

Iodine (*I*) is an essential trace element for all mammals. A lack of *I* leads to several *I* deficiency disorders (IDDs) such as goitre and cretinism (Gilfedder et al. 2010; Shetaya et al. 2012). In general, *I* concentrations in fresh waters and rocks are in the lower $\mu\text{g L}^{-1}$ range. The most important source of *I* to soils is the atmosphere. *I* compounds are released from seawater, transported in the atmosphere and deposited by wet or dry deposition to terrestrial and aquatic ecosystems. *I* accumulates in soils mainly through sorption to organic matter and to a lesser extent to sesquioxides and clay minerals. It is transported as iodide (I^-) or dissolved organic carbon (DOC)-complexes to groundwater and freshwater ecosystems.

According to previous studies, focused on boreal and temperate ecosystems, *I* can exist in several inorganic forms such as I^- , iodate IO_3^- , elemental iodine (I_2) and organically bound iodine. Due to the high affinity of *I* to organic matter, the ecohydrological behaviour of DOC largely controls the fate of *I* in soils and aquatic systems (Biester et al. 2004; Emerson et al. 2014; Gilfedder et al. 2010; Shetaya et al. 2012; Söderlund et al. 2011). The relationship between *I* and DOC in tropical soils, specifically the role of sorption to metal-oxides and/or DOM for the retention or mobilization of *I* in or from tropical soils are poorly understood. Compared to ecosystems of the temperate zones, tropical ecosystems are characterized by high temperatures, high precipitation, high weathering rates and high soil ages.

In this study, a tropical mountainous river catchment is investigated (“Alberto Manuel Brenes Biological Reserve” in Costa Rica) with the aim to decipher the relationship between *I* sorption in tropical soils-DOC-dynamics and release of *I* to an adjacent fluvial system.

Signature Prof. Dr. Harald Biester:

.....

Abstract

Iodine (*I*) is an essential trace element for all mammals. A lack of *I* leads to several health problems. Retention and mobilization of *I* in soils and related *I* loads in adjacent rivers in tropical ecosystems are poorly understood. The objective of the present study is to decipher soil-related factors that govern *I* retention and release dynamics in a tropical river catchment. Soil, river water and throughfall samples were taken in a pristine pre-montane rainforest in Costa Rica encompassing nine soil profiles, distributed equally in the catchments of two tributaries and the main river. River water was sampled over a period of five weeks. Solid phase sequential extraction was used to identify *I* binding-forms in soils. Further, streamflow was separated into baseflow (groundwater discharge) and quickflow (overland flow and interflow) to determine the flow path of precipitation and to investigate its influence on *I* release. Results showed, that *I* concentrations in soils were high (median: 69 mg kg⁻¹), but water-soluble fraction was on average 0.24 %, only. Low *I* mobility in soils leads to *I* concentrations between 0.77-1.26 µg L⁻¹ in stream waters during base- and even stormflow conditions. This indicates a strong sorption of *I* to the soil matrix. Solid phase sequential extraction identified *I* sorption to metal-oxides as the main retention factor (median: 79 % of total *I*). *I* is likely sorbed as *I*-DOC-complexes to metal-oxides. The separation of the streamflow into baseflow and quickflow revealed the dominance of baseflow and lower influence of activated shallow subsurface flow paths during rainfall events. Due to higher *I* concentration in throughfall compared to stream concentrations, it is likely that the soils of the catchment are not a source but rather a sink for *I*. Heavy rainfall events have only a very small influence on *I* mobilization. Groundwater discharge and to a lesser extent precipitation are the main *I* inputs to the streams in the catchment. In conclusion, tropical soils, rich in organic matter and sesquioxides, inhibit *I* release and support *I* accumulation through strong sorption.

Zusammenfassung

Iod (*I*) ist ein essentielles Spurenelement für alle Säugetiere und wird bei der Synthese von Schilddrüsenhormonen benötigt. Ein Mangel an *I* führt zu verschiedenen gesundheitlichen Problemen, unter anderem zu Kropfbildung oder Kretinismus. Mobilisierungs- und Retentionsprozesse von *I* in tropischen Böden und damit zusammenhängende *I*-Frachten in angrenzenden Flüssen sind nahezu unbekannt. Das Ziel der vorliegenden Studie ist es, bodenbezogene Faktoren zu analysieren, die die Retentions- und Freisetzungsdynamik von *I* in einem tropischen Flusseinzugsgebiet bestimmen. Kronendurchlass-, Fluss- und Bodenproben wurden in einem unberührten tropischen, premontanen Regenwald in Costa Rica entnommen. Die Bodenproben stammen aus neun Bodenprofilen, die gleichmäßig in den Einzugsgebieten der beiden beprobten Nebenflüsse und einem Hauptfluss angeordnet waren. Die Flusswasserproben wurden über einen Zeitraum von fünf Wochen entnommen. Eine sequentielle Festphasenextraktion wurde verwendet, um die *I*-Bindungsform in Böden zu identifizieren. Die Trennung der Abflussmengen des Hauptflusses in einen Basisabfluss (Grundwasserabfluss) und einen Direktabfluss (Oberflächenabfluss und Zwischenabfluss) dienen dazu, den Fließweg des Niederschlags zu bestimmen und deren Einfluss auf die Freisetzung von *I* zu untersuchen. Die Untersuchungen zeigten, dass die *I*-Konzentrationen in den Böden hoch sind (Median: 69 mg kg⁻¹), aber die wasserlösliche Fraktion im Durchschnitt nur bei 0.24 % lag. Die geringe *I*-Mobilität in Böden führt, während Basis- und Direktabfluss gleichermaßen, zu geringen *I*-Konzentrationen (zwischen 0.77-1.26 µg L⁻¹) in den benachbarten Flüssen. Dies deutet auf eine starke Sorption von *I* an die Bodenmatrix hin. Die sequentielle Festphasenextraktion identifizierte die *I*-Sorption an Metalloxide als Hauptretentionsfaktor (Median: 79 % von Gesamt-*I*). *I* wird wahrscheinlich als *I*-DOC-Komplex an die Oberfläche der Metalloxide sorbiert. Die Trennung in den Basisabfluss und den Direktabfluss, zeigte die Dominanz des Basisabflusses und den geringeren Einfluss von aktivierten oberflächennahen Strömungspfaden während starken Regenereignissen. Da die *I* Konzentrationen im Fluss während der gesamten Untersuchungszeit unter den Werten des Kronendurchlasses lagen, kann vermutet werden, dass die Böden des Einzugsgebietes keine Quelle, sondern eher eine Senke für *I* darstellen und Starkregenereignisse nur einen sehr geringen Einfluss auf die *I*-Mobilisation haben. Niederschlag, jedoch vor allem Grundwasserzufluss bilden die Haupteintragsquellen für *I* in die Flüsse. Damit hemmen tropische Böden, die reich an organischer Substanz und Sesquioxiden sind, die Freisetzung von *I* und unterstützen die *I*-Akkumulation durch starke Sorption.

1 Introduction

Iodine (*I*) is an essential trace element for all mammals, including humans and animals. A daily uptake by approximately 100 µg (Benoist 2004) is required by humans for a sufficient thyroid hormone production. An insufficient production can lead to a range of health risks including growth and development problems in children and goiter or cretinism in adults (Trotter 1960). These are collectively referred to as iodine deficiency disorders (IDDs). IDDs is a global health issue estimated to affect approximately 35 % of the world's population in 47 countries (Benoist et al. 2008).

I is present in all spheres; the hydrosphere, lithosphere, atmosphere and biosphere. In rainwater, *I* concentration ranges between 0.5-5.0 µg L⁻¹. Rivers and lakes worldwide contain *I* in the range of 0.5-20 µg L⁻¹ (Whitehead 1984), in non-arid regions between 1 and 10 µg L⁻¹ (Gilfedder et al. 2010) and average approximately 5 µg L⁻¹ (Yeager et al. 2017). But the majority (70 %) of *I* is retained in the ocean (Hou et al. 2009). Oceanic *I* compounds are released and transported in the atmosphere and deposited by wet and dry depositions to terrestrial and aquatic ecosystems (Shetaya et al. 2012). Due to the fact that the *I* content is generally significantly lower in rocks (0.08-0.50 mg kg⁻¹) than in overlaying soils (Whitehead 1984), the major source of *I* in soils is not weathering of bedrock but atmospheric deposition derived from the ocean. Therefore, *I* content in soils is higher near the coast (Fuge and Johnson 1986). Concentrations of *I* in soils vary between 0.5-20 mg kg⁻¹ (Fuge and Johnson 1986; Whitehead 1984) with a mean *I* concentration of 5 mg kg⁻¹ (Johnson 2003). In Northern Ireland in an organic-rich soil near the coast, concentrations up to 660 mg kg⁻¹ were found (Smyth and Johnson 2011). *I* is transported further inland through revolatilization-deposition processes of soils and aquatic systems (Yeager et al. 2017). *I* is volatilized mainly as methylated CH₃-*I* formed during biotic or abiotic degradation of organic matter (OM) (Amachi et al. 2001). Since atmospheric *I* is the major source, soils get enriched in *I* with soil aging and formation until the soil has reached the equilibrium concentration (Whitehead 1984).

Dissolution, complexation with dissolved components and colloid formation force *I* mobilization and migration (Renshaw et al. 2011). In aquatic systems, the main species are iodide (I^- ; -I), iodate (IO_3^- ; +V) and organically bound iodine (Org-I). In soils *I* exists dominantly as Org-I, in the form of colloidal particles or particulate matter, and to lesser extent as I^- and IO_3^- (Renshaw et al. 2011; Santschi and Schwehr 2004; Xu et al. 2011a; Yeager et al. 2017).

Many studies found soils as a main sink for *I* and underline the important role of SOM in *I* sorption due to Org-I formation and sorption of Org-I to soil particles (Dai et al. 2009; Fuge and Johnson 1986; Hou et al. 2003; Hou et al. 2009; Muramatsu et al. 2004; Schwehr et al. 2009; Shetaya et al. 2012; Whitehead 1973, 1984; Xu et al. 2011a; Yeager et al. 2017; Yoshida et al. 1992). This can be ascribed to the biophilic nature of *I* (Santschi and Schwehr 2004). The capacity of OM to sorb *I* increases under aerobic conditions (Kodama et al. 2006) and as decomposition progresses (Whitehead 1974). *I* sorbs to decomposed, humified OM, but not to fresh OM (Muramatsu et al. 2004). The direct sorption of *I* to mineral facies, such as oxides and hydroxides of iron (Fe_2O_3) is less important (Yeager et al. 2017); even in soils with low SOM content (Hu et al. 2009; Xu et al. 2015).

1.1.1 Mechanisms of Iodination

OM is halogenated abiotically (Steinberg et al. 2008a) or biotically (Yeager et al. 2017). Several previous studies pointed out the importance of biological activity, enzymes and plant exudates in *I* speciation and in particular in the *I* redox cycle (Fig. 2) and therefore in the fixation of *I* (Grimvall et al. 1994; Söderlund et al. 2011; Yeager et al. 2017). Especially enzyme-catalysed reactions enhance iodination of SOM (Amachi 2008; Li et al. 2011; Santschi and Schwehr 2004; Yeager et al. 2017) with higher rates at pH values above 5 (Yeager et al. 2017), as well as under aerobic conditions. During I^- oxidation to IO_3^- and vice versa IO_3^- reduction to I^- intermediate species (I_2 , hypoiodous acid (HIO) and triiodide (I_3^-)) are formed (Bowley et al. 2016; Li et al. 2011; Yeager et al. 2017; Zhang et al. 2011). Perhaps the best-known halogenating enzymes are haloperoxidases (HPOs). HPOs utilize hydrogen peroxidase (H_2O_2) as a cosubstrate to catalyse the oxidation of halide ions (I^-) to hypoiodous acids (HOI) (Leri and Myneni 2012; Li et al. 2011; Yeager et al. 2017).

The oxidized *I* species (HOI, I_2 , I_3^-) are strong electrophiles intensifying the reaction with SOM (Bowley et al. 2016; Li et al. 2011; Yeager et al. 2017; Zhang et al. 2011) and can replace -H with -*I* (electrophilic substitution) in aromatic rings or organic moieties (including phenol, polyphenols, quinones or alkenes) to form a stable organo-iodine bond (Li et al. 2011; Shetaya et al. 2012).

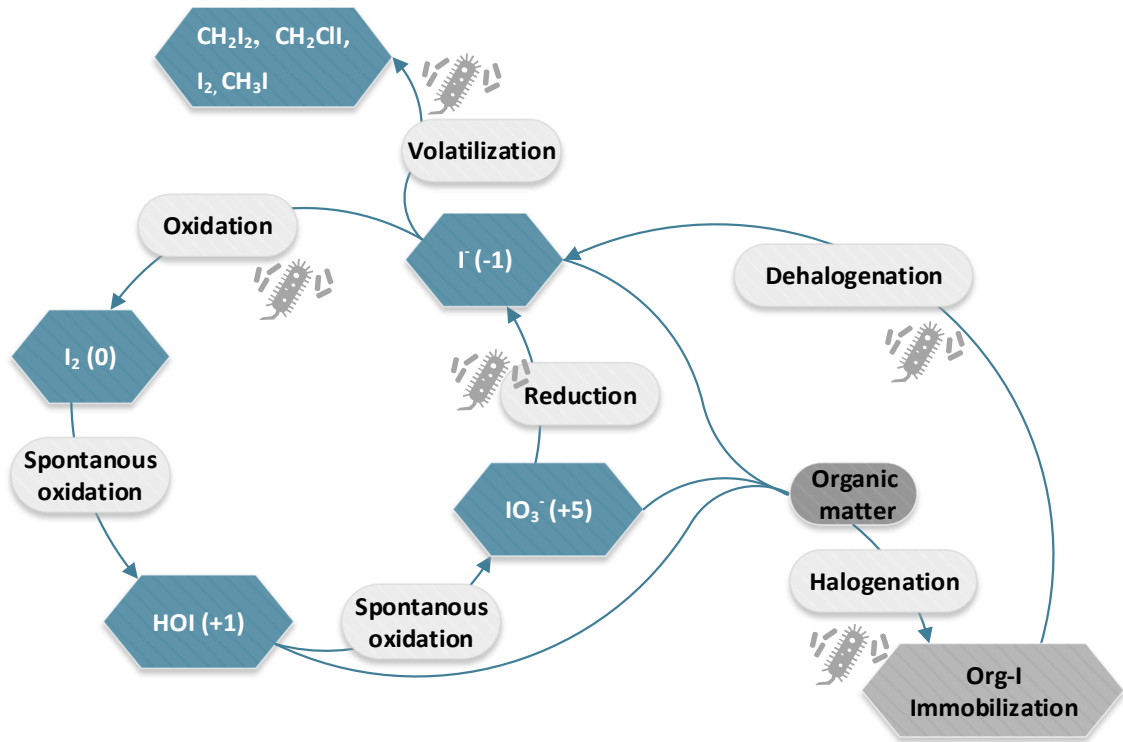


Figure 2 Schematic iodine redox cycle (adapted from Amachi (2008); Yeager et al. (2017)).

The most important organic compounds associated with *I* are probably aromatics, especially humic substances formed during decomposition (Whitehead 1974; Yeager et al. 2017; Zhang et al. 2011). Aromatics are characterized by conjugated double bonds, which facilitate *I* bonding and the conversion to organo-*I* species via stable covalent binding (iodination) (Bowley et al. 2016; Muramatsu et al. 2004; Shetaya et al. 2012; Smoleń et al. 2016; Zhang et al. 2011). Therefore, soils rich in OM retain more *I* than soils with less OM (Dai et al. 2009; Shetaya et al. 2012; Shimamoto et al. 2011). On the other hand, dehalogenation takes place simultaneously by abiotic and biotic processes due to mineralization of organohalogens (Martínez-Cortizas et al. 2016).

Without microbiological activity I^- is transformed to Org-*I* to a lesser degree (Yeager et al. 2017). In acidic soils (pH <5) abiotic iodination is more important (Yeager et al. 2017).

1.1.2 Sorption to inorganic components

Sorption of *I* is linked to opposite charged surfaces of soil components (Kaplan et al. 1995). Anionic *I* species (I^- and IO_3^-) may sorb to positively charged surfaces of soil components that can be found on clays (2:1 and 1:1), Fe-oxides and OM (carboxyl groups of OM) (Kaplan 2003; Yoshida et al. 1992). The number of positively charged surface sites is influenced by the pH conditions (Hu et al. 2009; Li et al. 2014). Under pH conditions above the point of zero charge

(pH_0 where the net surface charge is 0 meq kg^{-1}) (Kaplan 2003), most soil minerals have net negative charges, because protons on the surface of these minerals desorb and are replaced by hydroxyl ions. This leads to electrostatic repelling of anionic I^- species (for instance I^- and IO_3^-) (Kaplan et al. 1995). With a pH decreasing below the point of zero charge, mineral surfaces become more positively charged because solved protons sorb to functional groups of the minerals surfaces, and may electrostatically attract anions (Koch-Steindl and Pröhl 2001). The point of zero charge for silicates and 2:1 minerals is around 2.5, for kaolinite 4.6, for Fe-oxyhydroxides 6 - 8, and for gibbsite 5 (Kaplan 2003).

I^- is mainly sorbed to OM under alkaline conditions ($pH > 6$), whereas under more acidic conditions metal-oxides become the major adsorbing constituent (Whitehead 1973). Especially IO_3^- is retained via sorption to inorganic components (Couture and Seitz 1983; Hu et al. 2005; Hu et al. 2009; Shetaya et al. 2012; Yoshida et al. 1992). It shows higher and stronger sorption to several minerals and lower solubility under aerobic conditions in comparison to I^- (Couture and Seitz 1983; Dai et al. 2009; Hu et al. 2005; Kaplan 2003; Kodama et al. 2006; Ootosaka et al. 2011; Shetaya et al. 2012; Shimamoto et al. 2010; Shimamoto et al. 2011; Yoshida et al. 1992).

It is presumed that differences in sorption behaviour between IO_3^- and I^- are caused by “the harder base nature of IO_3^- ” which would result in “hard-hard interactions with the hard acid sites on the mineral surfaces” (Kaplan 2003). IO_3^- is probably adsorbed by mechanisms similar to that of other oxyanion adsorption to ferric hydroxide like phosphate (Kaplan 2003; Yoshida et al. 1992). The sorption based on ligand exchange (chemically adsorption) and the displacing of surface OH^- of allophane and sesquioxides leading for example to the formation of $Fe-OIO_2$ bonds (Couture and Seitz 1983; Kaplan 2003; Yoshida et al. 1992).

I^- adsorption is mainly influenced by the cation exchange capacity (CEC) and the content of OM (Shetaya et al. 2012; Whitehead 1973). The retention of I^- is primarily attributed to weak physisorption (adsorption) to OM (Dai et al. 2009; Shetaya et al. 2012). Therefore, soils high in OM content and high CAC have a high potential to retain I^- . But Dai et al. (2009) also demonstrated that OM and CEC only explained less than half of the variation in I^- adsorption. They concluded that there are some undefined factors such as clay minerals and soil texture controlling I^- sorption in soils.

However, also I^- may sorb to freshly precipitated hydrated Fe-oxides at pH values below 5 (Whitehead 1974). The sorption of I^- to allophanes and/or sesquioxides is based mainly on electrostatic adsorption on positive charged surfaces influenced by pH (Yoshida et al. 1992). Thus, sorption ability decreases as pH increases (Whitehead 1973).

1.2 Forested mountain watersheds in the tropics

I cycling, mobility and availability for biological uptake is influenced not only by *I* binding-forms in the soil (Li et al. 2013) but also by the hydrology of the catchment including hydrological flow paths and intensity of rain (Hope et al. 1994; Moore 1989).

According to Dissanayake and Chandrajith (1999) mountainous areas with high and extreme rainfall events and drought are likely to be depleted in *I* due to intense leaching. In contrast, a study by Muramatsu et al. (2004) revealed that regions high in precipitation (andosols in a small island in Kyushu, Japan) exhibit high sorption of *I* and low *I* solubility in water and thus low bioavailability and plant uptake (Whitehead 1984).

Hydrological processes differ between temperate and tropical catchments (Cheng et al. 2017). Tropical climates are characterized by constant high temperatures (Cheng et al. 2017), higher annual rainfall amounts and frequency, greater energy input (Scholl et al. 2015), high biological activity (Crespo et al. 2011), high soil ages and tree density. These factors leading to higher weathering rates of the bedrock (Cheng et al. 2017; Scholl et al. 2015), highly weathered soils, the formation of deep saprolitic (Cheng et al. 2017) or clayey soils (Scholl et al. 2015) and preferential flow paths caused by macro- and microorganisms (Cheng et al. 2017). Together they determine the runoff generation and partitioning of rainfall into different hydrologic flow paths (Fig. 3) (Cheng et al. 2017; Elsenbeer et al. 1995). Effects of tropical conditions on *I* retention and mobilization and related *I* loads in adjacent rivers are poorly understood.

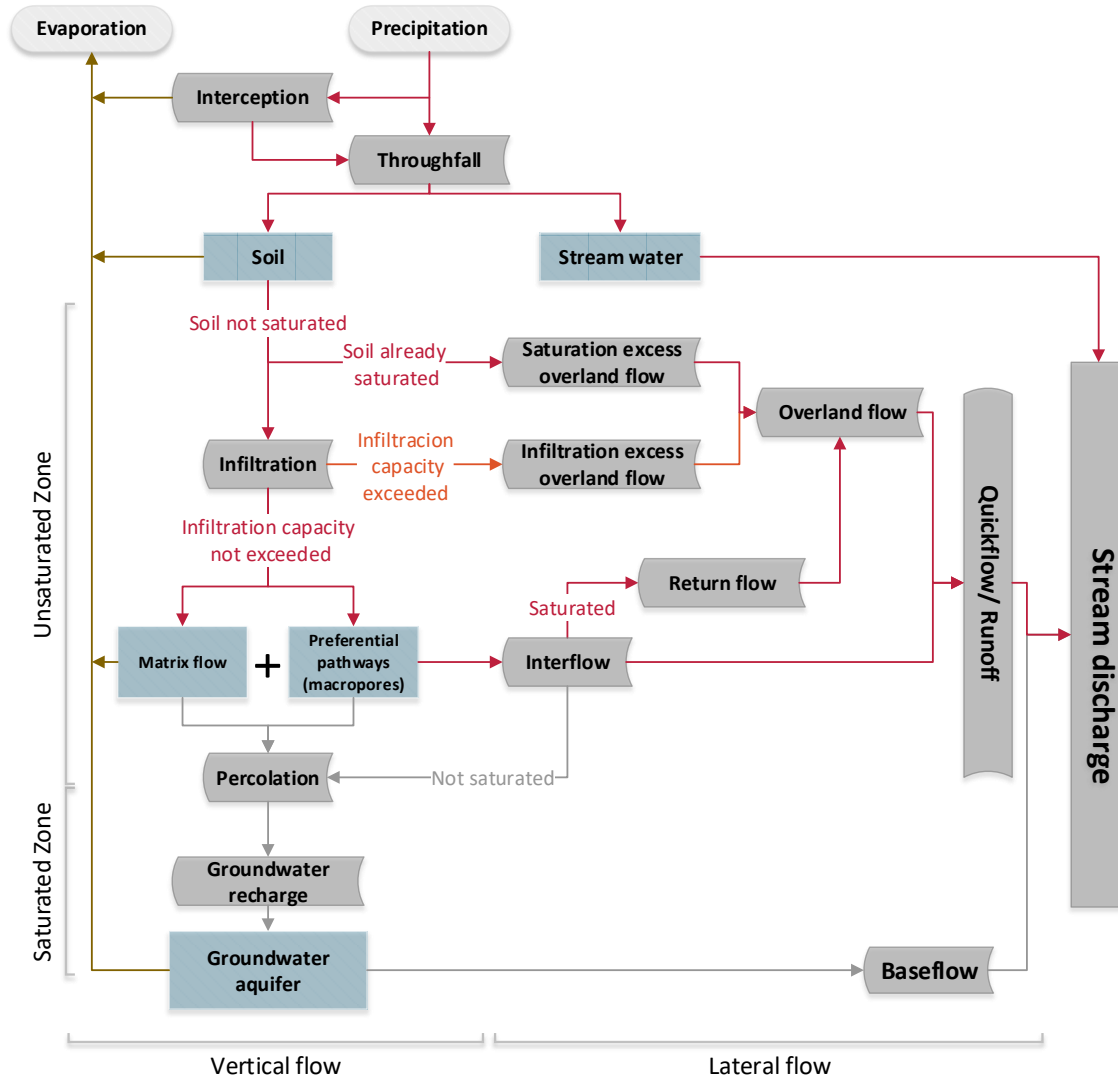


Figure 3 Hydrological pathways. Groundwater and baseflow pathways are shown in grey, stormflow pathways in red (including saturation excess flow), infiltration excess pathways in orange, evapo(transpiration) in dark yellow (adapted from Cheng et al. (2017)).

Streams are composed to a varying extent of baseflow and quickflow depending on antecedent conditions (Zimmer and McGlynn 2017). In general, baseflow is discharged with long-term delay from groundwater storages as groundwater runoff. Quickflow is the short-term response of a rainfall event and occurs during stormflow. The quickflow consists of two main components; the lateral subsurface flow in the soil profile (interflow) and the overland flow (Welderufael and Woyessa 2010; Zimmer and McGlynn 2017). Overland flow occurs when rainfall intensity is greater than the infiltration capacity (infiltration excess overland flow), if the soil is already saturated and incoming rainwater falls directly onto this area and cannot infiltrate (saturation excess overland flow) or groundwater or interflow water seeps out from the subsurface and generate overland flow (return flow) (Crespo et al. 2011; Sklash et al. 1986).

During rain events, 50 % canopy interception loss is assumed. Thus, only half of the rainwater reaches the forest soil as canopy throughfall (Elsenbeer et al. 1995; Scholl et al. 2015). Canopy throughfall is either entering the stream channel directly, falls onto the soil and infiltrates into the soil or discharges as saturation excess overland flow into the stream (Fig. 3). In general, undisturbed tropical rain-forests exhibit high soil infiltration rates (Elsenbeer et al. 1995) due to a high density of macropores forming preferential flow paths (PFPs) (Cheng et al. 2017). Macropores result from the activity of soil fauna, root growth and decay and the shrinking of clay. PFPs enable a fast flow path to stream channels (Schellekens et al. 2004). PFPs in vertical and horizontal direction play an important role in catchment hydrology, contribution to runoff and groundwater recharge and thus in the baseflow composition (Cheng et al. 2017; Schellekens et al. 2004). It was found that stemflow also contributes to the macropore flow as water flowing down the stem of a tree is accumulating at the tree stem-soil interface, the starting point of roots (Cheng et al. 2017)

Infiltration capacities are dependent on soil types and vegetation cover. (Crespo et al. 2011; Sklash et al. 1986). The high density of trees preserve the soil structure and functions and prevent high overland flows and hence high soil erosion (Scholl et al. 2015). Thus, in tropical catchments PFPs cause higher infiltration and absorption of throughfall compared to those in temperate regions and lead to diminished overland flow (Cheng et al. 2017) and intensify recharge of groundwater and storage during dry seasons.

To analyse if rainfall events affect the export of I into the stream and the more influential component on the streamflow, a separation into baseflow and quickflow is necessary (Welderufael and Woyessa 2010). Further, a chemical consideration will be used to identify flow generation zones to determine the preferential pathway in which I is transported into the stream and the influence of the catchment hydrology on I discharge.

The objective of the present study is to decipher soil-related factors that dominate I retention and release dynamics in an old tropical river catchment. Soil and water samples were taken in a pristine pre-montane rainforest in Costa Rica encompassing nine soil profiles, distributed equally in the catchments around two tributaries and the main river. River water was sampled over a period of five weeks. In addition to I concentrations in stream water, a solid phase sequential extraction was conducted to identify I binding-forms in the soil.

2 Materials and Methods

2.1 Study site

The San Lorencito headwater catchment is situated in the Atlantic slope central Volcanic Cordillera in Costa Rica (Central America). The catchment is part of the Alberto Manuel Brenes Biological Reserve (ReBAMB) encompassing 3.2 km² pristine pre-montane rainforest with an altitude ranging between 890 and 1450 m. It is characterized by deeply incised V-form valleys, highly dynamic streams and steep slopes of around 17°. The tertiary tropical volcanic parent rock material consists mainly of andesite and basalt. In between five to nine million years a deep, weathered regolith and an overlying old, porous loamy soil of andosol type has developed.

The predominant climate in this region is tropical rainforest climate with an average annual temperature of about 21 °C, a mean precipitation of 3589 mm yr⁻¹, a potential evapotranspiration of around 849 mm year⁻¹ with little seasonality and a relative humidity of constantly 98 %.

The study area of the San Lorencito stream is divided into one main channel (Q_M) with a length of 3.2 km and a mean river slope of 6.3°, and two tributaries, each on one catchment side of the main stream (Fig. 4). Looking upstream the tributary on the right side (Q_R) encompassing a catchment area of 0.21 km² (C_R) and the tributary on the left side (Q_L) encompassing a catchment area of 0.15 km² (C_L). The mean slope of C_L and C_R is nearly the same around 16.5° (C_R : 16.8°, STD: 20.57 %; C_L : 16.4°, STD: 19.91 %). But maximum values differ in C_L and C_R . C_L exhibit a higher maximum slope (68.3°) than C_R (63.0°).

The surrounding flora and fauna is high in endemic species. The maximum vegetation height is 50 m.

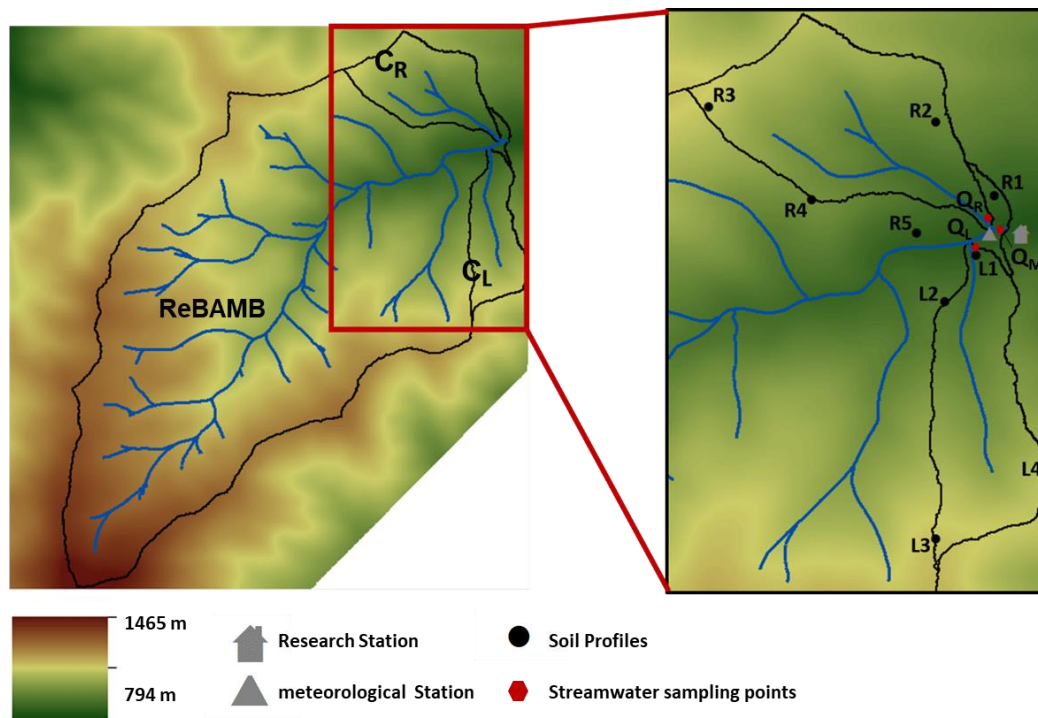


Figure 4 Left: Overview of the San Lorencito catchment, ReBAMB, Costa Rica. Right: Enlarged section (main study area) of the ReBAMB: locations of soil profiles (black points) in the catchments on the right side C_R and the left side C_L ; sampling points for stream water (red pentagons) of the two tributaries (Q_R ; Q_L) and the main stream (Q_M), the research (grey house) and meteorological station (grey triangle). The boundaries of the catchments (ReBAMB, C_R and C_L) are shown in black.

2.2 Study and sampling design

2.2.1 Sampling of soil

Within the study area, nine soil profiles were distributed equilibrated around the tributaries, five within C_R (R1-R5) and four within C_L (L1-L4). The profile depth was 0.5 m-0.6 m with a width of around 0.7 m. One soil profile with a depth of approximately 1 m was established in C_R (R2) and C_L (L2), respectively.

Physical soil properties for each layer were recorded in the field including thickness of soil layers, soil depth, aggregate type, Munsell colour, degree of rooting and skeleton, texture, pore volume, activity of macro-fauna and soil type. The latter one was defined according to the World Reference Base for Soil Resources (WRB) (IUSS Working Group 2014).

To measure I content in the soil horizons, approximately 0.5 kg of disturbed soil material from each soil horizon was collected on four days in June 2017, at the beginning of the rainy season.

All soil samples were taken in the middle of each soil horizon and collected in plastic bags (Whirl Packs). They were collected by hand, wearing gloves to avoid contamination.

The soil samples were stored in a refrigerator (4 °C) and shipped to Germany for analyses. Before analyses, samples were oven-dried at 40 °C for three days and homogenized by passing the soil samples through a 2 mm sieve.

2.2.2 Sampling of stream water

Three representative measuring points were selected to measure the total discharge of each tributary and of the main channel and to take samples of biofilms (biological deposits) deposited on the surface of rocks in the river bed.

In May and June 2017 grab samples were taken of the discharge of Q_M , Q_L and Q_R every second day or even daily in four intervals each of three till five days. Samples were taken with 50 ml PE bottles, which were rinsed with sample water before sampling. Q_M was sampled up to three times a day by an automated water sampler (ISCO 3700, Teledyne). Directly before each discharge water sampling the hose (Teflon) was rinsed automatically with sample water. The frequency and duration of each interval was dependent on accessibility of the study site and intensity of rain events. The total period of sample collection was approximately five weeks.

Temperature, pH, redox potential (Eh), conductivity (EC), total dissolved solids (Tds) were measured in-situ by using a handheld Hanna multi-parameter probe (HI 98195). Discharge was measured using a digital water velocity meter (FP111 flow probe; Global Water). All these parameters were measured at the time of sample collection.

Water samples were vacuum filtered (<0.45 μm) using a nylon filter, stored in a freezer (-18 °C) and were shipped frozen to Germany.

2.2.3 Sampling of stream biofilms

Biofilm material was collected one-time in Q_M , Q_L and Q_R using a 300 ml suction plastic pump, which were rinsed with stream water before sampling. The suspension was decanted from the suspended material, frozen, dried at 40 °C and ground in a mixer mill (MM 301, Retsch GmbH, Hahn Germany).

2.2.4 High-resolution stream and climate data

In addition, water level, turbidity, water temperature, stream pH were obtained from a multi-sensor box at Q_M (Water Quality Monitoring System; Global Water). Precipitation, air

temperature, relative humidity, solar radiation data were obtained from a meteorological station at 1171 masl (climate monitoring station; Global Water). Both were recorded at five minutes intervals during the entire sampling period.

2.2.5 Sampling of canopy throughfall

Canopy throughfall accumulated in a precipitation gauge (Rain sampler RS-1B, Palmex-Zagreb, No 2404/15) during one week (07.-14.06) was taken one-time. The sample was vacuum filtered ($<0.45\ \mu\text{m}$) using a nylon filter, stored in a freezer ($-18\ ^\circ\text{C}$) and was shipped frozen to Germany.

2.3 Chemical analysis

2.3.1 Soil analysis-sequential extraction of iodine

To differentiate between various forms of *I* in soil, a sequential extraction procedure according to Schmitz and Aumann (1995) was conducted with soil samples of the profiles L1, L3 as well as R1, R3 and R5. The method consists of five main steps with five different solutions and distinguishes between four possible associations of *I*; water-soluble *I*, exchangeable *I*, *I* adsorbed on metal-oxide surfaces and Org-*I*.

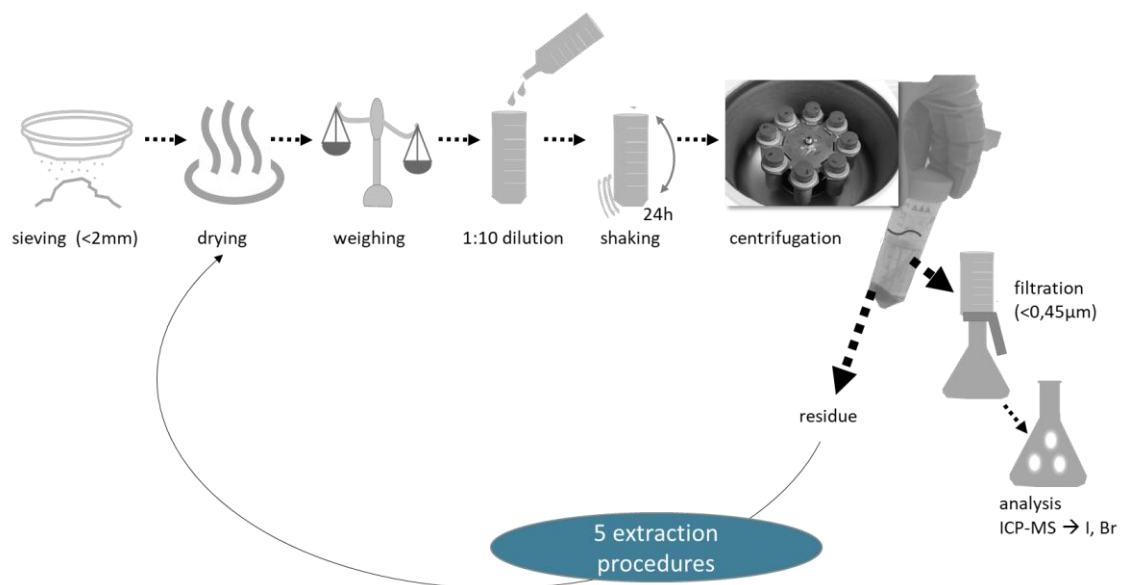


Figure 5 Schematic procedure of each sequential extraction step for iodine fractionation in soil.

After the soil samples were dried at $40\ ^\circ\text{C}$ for three days on plastic plates, sieved to $<2\ \text{mm}$ and homogenized, a subsample of $0.025\ \text{kg}$ was taken (Fig. 5).

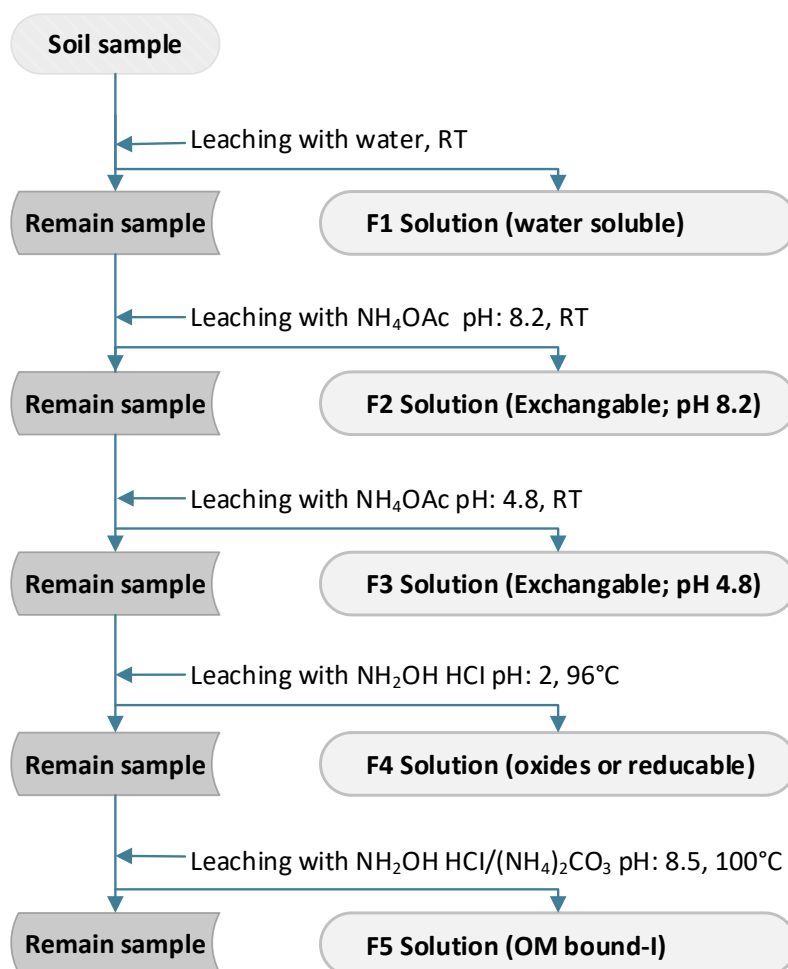


Figure 6 Schematic diagram of the sequential extraction procedure for iodine fractionation in soil samples.

The first extraction step was the extraction of water-soluble *I* with water (F1). The exchangeable *I* was extracted in two consecutive steps using the same reagent at different pH values. Both steps were carried out with 1 molar ammonium acetate (NH_4OAc) solution. In the first step, ammonium (NH_4) was pipetted to reach pH 8.2 (F2). In the second step, acetic acid (AcOH) was pipetted to reach pH 4.8 (F3). According to Hou et al. (2009) F3 extracts *I* associated with carbonates.

To release adsorbed *I* on metal-oxide surfaces, reducing conditions are required. In the fourth extraction step the soil samples were extracted with 0.04 molar hydroxylammonium chloride ($\text{NH}_2\text{OH HCl}$) dissolved in 25 % (v/v) AcOH solution (F4). To reach pH 2, AcOH was added.

The last extraction step targeting *I* bound to OM has been carried out using a mixture of hydroxylamine and sodium carbonate solution ($\text{NH}_2\text{OH HCl}/(\text{NH}_4)_2\text{CO}_3$) because of its oxidative

strength (F5). The reagent was deacidified by adding NH_4 to reach a pH value between 8 and 9 (here: 8.5).

The soil samples were extracted using a soil/solution ratio of 1:10. The suspension was shaken moderately for 24 hours prior to separation by centrifuging and subsequent decantation (Fig. 5). Extraction F1-F3 was shaken at room temperature (RT), extraction F4 at 96 °C and F5 at 100 °C. The residue after each separation was dried and used for the next extraction step (Fig. 6)

The leachates were vacuum filtered (<0.45 μm) using a nylon filter, stored in a freezer (-18 °C).

2.3.2 Water analysis

DOC was determined by thermo-catalytic oxidation with multi N/C 2100 after acidification of the samples with 1 v/v HCL (37 %) to a pH of 2 to remove inorganic carbon. Measurements of DOC were validated by comparison to certified reference samples (Mauri 09 and TOC20 reference).

The concentrations of dissolved anions chloride (Cl^-), nitrate (NO_3^-), sulphate (SO_4^{2-}) in the water samples were determined by ion chromatography (IC; 761 Compact IC) using 10 ml of samples. The quality of the measurements was controlled by certified reference material (Sigma-Aldrich QC1364) and standard stock solution (Fluka54704).

After acidification to approximately pH 2 by adding 1 v/v nitric acid (HNO_3 ; 60 %) calcium (Ca), potassium (K), magnesium (Mg), sodium (Na), zinc (Zn) were measured using inductively coupled plasma atomic emission spectroscopy (ICP-AES, Varian 715-ES). For the evaluation of the precision and accuracy of the measurement, a certified reference material (River Thames LGC6019) was used.

Further major and trace element concentrations (argon (Ag), arsenic (As), barium (Ba), beryllium (Be), bismuth (Bi), boron (B), cadmium (Cd), cerium (Ce), chromium (Cr), copper (Cu), Fe, lanthanum (La), lead (Pb), lithium (Li), manganese (Mn), molybdenum (Mo), nickel (Ni), rubidium (Rb), scandium (Sc), selenium (Se), strontium (Sr), thallium (Tl), titanium (Ti), uranium (U), vanadium (V), yttrium (Y) and zirconium (Zr)) were determined by means of ICP-MS (Agilent 7700; Germany) in acidified samples by adding 1 v/v nitric acid (HNO_3 ; 60 %). The quality of the measurements was controlled by certified reference material (River Thames LGC6019 and SPS-SW1).

Concentrations of *I* and bromine (Br) were analysed by ICP-MS. The quality of the measurements was controlled by certified reference material (Roth and Fluka54704).

All measurements of *I*, Br and the anions (except SO_4^{2-}) were in the range of the certified values. DOC and Sc, Ni, Se, Rb, Sr, Y, Mo, Cd, Ba, La, Ce, Tl, Pb and U analyses showed small deviations from certified values. For measured values and certified values of the references see Table 9 and 10 in the appendix.

2.3.3 Solid analysis

Solid samples comprised biofilm samples and parent rock samples.

Fe, K, aluminium (Al), silicon (Si), sulfur (S), Ca, Y, Zr were determined using an energy-dispersive x-ray fluorescence spectrometer (XRF; self-construction at TU Braunschweig). The quality of the measurements was controlled by certified reference material (LKSD4).

To determine *I* and Br content in the solid samples, *I* was trapped in water by thermal extraction using an AOX analyser (Thermo Euroglas AOX). Followed by the determination of *I* using ICP-MS. The quality of the measurements was controlled by certified reference material (China sediment 73312 and China soil DC73030).

Measured values of *I* and Br were in the range of the certified values of the China Sediment reference but showed deviations from certified values of the China Soil reference. XRF measurements showed deviations from certified values in the LKSD4 reference for S, Si, K, Zr. For measured values and certified values of the references see Table 8 in the appendix.

2.4 Calculation

2.4.1 Load and flux calculation

Element loads were determined by the product of the discharge measurements ($\text{m}^3 \text{s}^{-1}$) and corresponding measured instantaneous element concentrations, for example *I* ($\mu\text{g L}^{-1}$), in water samples. The values of the calculated loads were divided by the corresponding catchment size to obtain element fluxes ($\mu\text{g s}^{-1} \text{ km}^{-2}$).

2.4.2 Classification of precipitation

Table 1 Classification of rainfall events based on daily intensity

Rainfall event	Intensity [mm d ⁻¹]
No rain	0-1
Light rain	1-5
Moderate rain	5-20
Heavy rain	20-40
Violent rain	> 40

In order to group the rainfall events the classification by Zambrano-Bigiarini et al. (2017), based on daily intensity, was used (Tab. 1). They have therefore modified the values from the World Meteorological Organization (2008).

2.4.3 Streamflow separation

Baseflow and stormflow separation was conducted by the recursive digital filter technique (RDF-method) after Arnold and Allen (1999). It is the most widely used separation method based on a filtering procedure. First, the quickflow was separated from total streamflow with the filter equation:

$$DQ_{(t)} = \alpha DQ_{(t-1)} + \frac{1+\alpha}{2} (Q_{(t)} - Q_{(t-1)}) \quad (\text{Eq. 1})$$

$DQ_{(t)}$ filtered quickflow at the t time step

$$DQ \geq 0$$

$Q_{(t)}$ total original streamflow (baseflow + quickflow)

α filter parameter, here 0.925 determined by Nathan and McMahon (1990)

Secondly baseflow, BQ, was estimated by using the equation

$$BQ_{(t)} = Q_{(t)} - DQ_{(t)} \quad (\text{Eq. 2})$$

2.4.4 Enrichment factor

To identify differences in mean element concentrations or fluxes in stream water during baseflow and quickflow conditions and between C_L and C_R , enrichment factors as division of the respective mean values were calculated. Results are pictured as bar diagrams and illustrate increasing or decreasing element concentrations or fluxes. This helps to identify flow generation zones and differences between C_L and C_R . The goal is to determine the preferential pathway of I transport to the stream and the influence of the catchment hydrology on I discharge.

Further enrichment factors of I compared to Br were obtained by division of mean I and Br concentrations and expressed as I:Br-ratios.

2.5 Statistical analysis

To identify relations between streamflow discharge and solute-concentrations, correlation coefficients were calculated. Every correlation coefficient was calculated by the spearman method. The correlation coefficient by Spearman (r_s) is suitable for non-linear relations between two variables, which is appropriate for these variables (Dupas et al. 2017)

All statistical analyses and plots were performed using the statistical program R 3.2.1 (R Development Core Team 2015) except for the average, median, standard deviation, minimum and maximum values calculated using Excel (Microsoft Office, 2013). Schematic diagrams were visualized by Visio (Microsoft Visio Professional, 2013) or PowerPoint (Microsoft Office, 2013). Geographical investigations and visualizations of the study area were conducted using ArcGIS 10.5.

3 Results

3.1 Sequential extraction

The measurement of the *I* binding-forms in the soil yielded results for the first four extraction steps. During the last extraction procedure, the vessels opened in the oven during shaking and the solution evaporated. A possible reason could be too high temperatures in combination with the extraction solution leading to too high pressure in the vessels. The possible amount of *I* extractable during the last step was determined indirectly by subtraction of the sum of the amount of *I* extracted during F1-F4 from the total amount of *I* in the solid soil samples. The total amount of *I* in the soil samples was measured in a parallel study by Schulz (2018) conducted in the same study area in freeze-dried and ground samples. As described in section 2, soil samples were oven-dried and sieved to <2 mm for the extraction procedure. Which is probably the main reason why the determined sum of *I* content extracted during F1-F4 are higher than the values of the total *I* content in some soil samples. Consequently, extractable *I* in percentage of total *I* in the solid soil may reach values higher than 100 % (Fig. 7).

3 Results

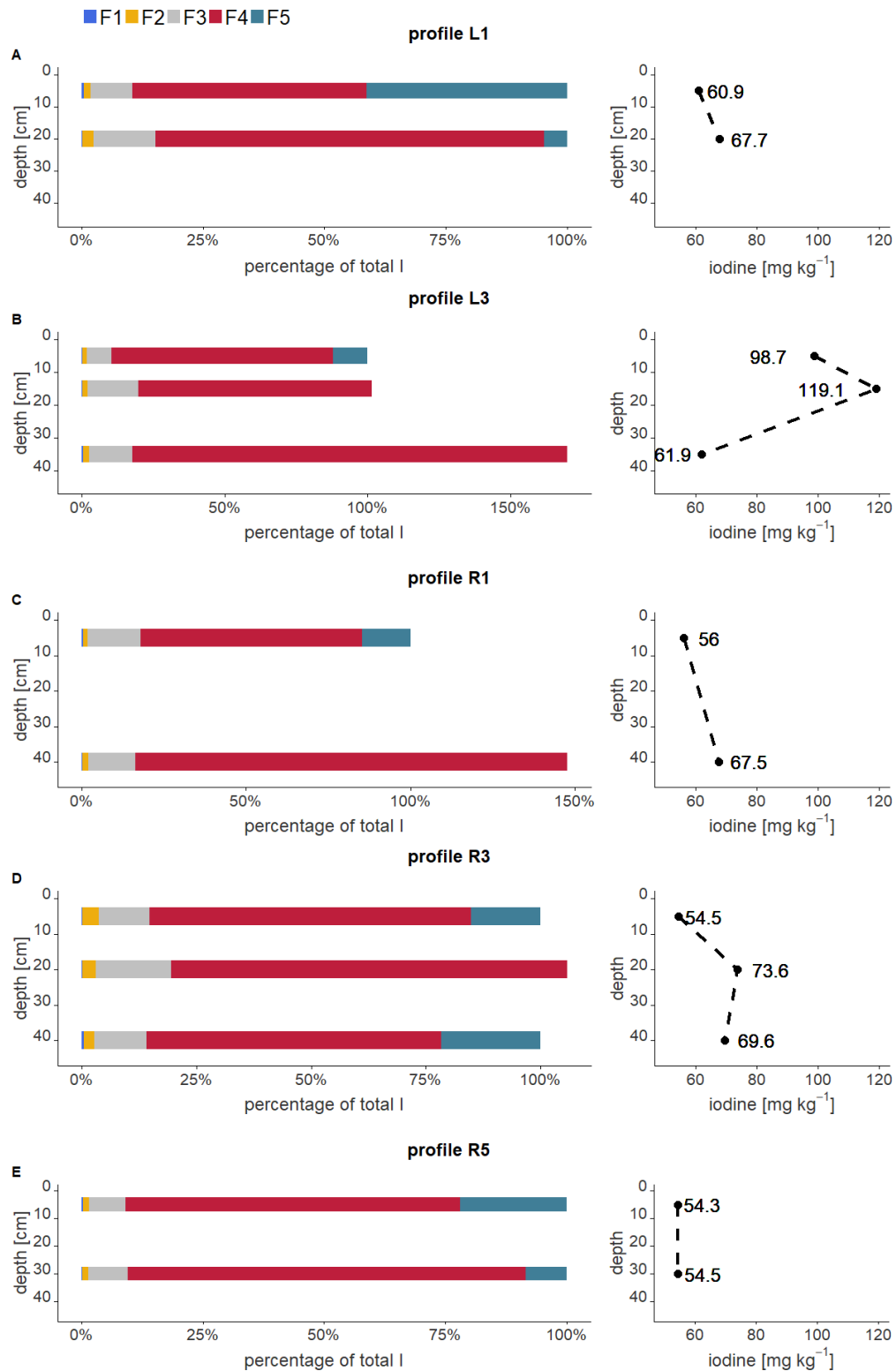


Figure 7 Left: Extractable iodine concentrations [mg kg^{-1}] in percentage of total iodine amounts in the respective soil horizon [%] of each extraction step F1-F5 in profiles L1 (A), L3 (B), R1 (C), R3 (D), R5 (E). Right: Total iodine concentration in soil profiles (measured by Schulz (2018)).

On average, only 0.2 % of total *I* [F1-*I*%] was water extractable. In soil profiles sampled in three depths (L3, R3), results showed higher water solubility in the topsoil horizons (5 cm) and the subsoil horizons (> 20 cm). In soil profiles sampled in two depths only (L1, R1, R5), a decrease in water soluble *I* was found. A higher C:N-ratio in solid samples (Schulz 2018) reduce [F1-*I*%] ($r_s = -0.57$, $p = 0.05$) and also total water leachable *I* amounts [F1-*I*] ($r_s = -0.43$, $p = 0.16$) (Tab. 2).

On average, 2 % were extractable at pH 8.2 [F2-*I*%] and 12 % at pH 4.8 [F3-*I*%]. In both extractions, *I* was to a greater extent extractable at a depth of around 15-20 cm (L1, L3, and R3) or in subsoil horizons (R1). At the same depth water extractable *I* was decremented. In profile R5 a decrease in [F2-*I*] was found.

The major amount of *I* was extracted during the fourth step (reducing step), the extraction of *I* bound to metal-oxide surfaces. An average of 67 % of total *I* [F4-*I*%] in the upper 5 cm, 83 % in the range of 15-20 cm and 107 % in the deeper horizons between 30-40 cm was extracted. [F4-*I*] increased with soil depth ($r_s = 0.52$, $p = 0.09$). Furthermore, the more clay minerals ($r_s = 0.57$, $p = 0.05$), exist in the soil the more [*I*] was extracted during F4. [F4-*I*%] was significantly positive correlated with Si ($r_s = 0.61$, $p < 0.05$) and positive with increasing depth ($r_s = 0.55$, $p = 0.06$).

The indirect determination of *I* bound to OM [F5-*I*] revealed a great variability in values. [F5-*I*%] values ranged between - 47.7 % and 41.4 % and need to be carefully considered. Nevertheless, a negative correlation between [F5-*I*] with depth ($r_s = -0.52$, $p = 0.085$) was determined.

Table 2 Spearman correlation coefficients of I in mg kg⁻¹ [I] and I in percent [%] of the extraction procedures with depth, soil texture and other element concentrations measured by Schulz (2018). Non-significant correlations are marked in grey

	F1		F2		F3		F4		F5	
	[I]	I [%]	[I]	I [%]	[I]	I [%]	[I]	I [%]	[I]	I [%]
depth	0.03	0.07	0.08	0.26	0.34	0.28	0.52	0.55	-0.52	-0.58*
clay	0.10	-0.04	0.42	0.30	0.24	0.17	0.58	0.35	-0.22	-0.37
silt	-0.05	-0.25	0.47	0.26	-0.09	-0.15	0.05	-0.17	0.32	0.18
sand	-0.04	0.25	-0.60*	-0.36	-0.26	-0.14	-0.51	-0.17	0.03	0.23
I	-0.13	-0.50	0.76**	0.46	0.71*	0.56	0.67*	0.22	-0.19	-0.42
C	-0.15	-0.34	0.13	-0.20	-0.04	-0.05	-0.21	-0.45	0.41	0.39
C:N	-0.43	-0.57	0.25	0.02	0	-0.04	-0.06	-0.27	0.24	0.21
Fe	0.29	0.28	0.22	0.19	0.34	0.36	0.38	0.32	-0.34	-0.32
Si	-0.20	0.07	-0.11	0.27	0.07	0.07	0.28	0.61*	-0.59*	-0.53
Mn	0.18	0.06	-0.29	-0.51	-0.25	-0.36	0.16	0.21	-0.01	-0.04
N	0.17	-0.03	-0.19	-0.52	-0.26	-0.27	-0.38	-0.50	0.55	0.52
Zr	-0.03	0.11	0.63*	0.87***	0.43	0.52	0.25	0.21	-0.30	-0.31
Sr	-0.36	-0.17	-0.59*	-0.59*	-0.41	-0.40	-0.52	-0.13	0.15	0.29

P < 0.05, **P < 0.01, ***P < 0.001

3.2 Catchment hydrological data

3.2.1 Frequency distribution of rainfall intensity

Based on WMO classifications there were 5 days with no and also 5 days with light rainfall (Fig. 8), 13 days with moderate, one day with heavy and one with violent rain intensity during the sampling period. The heavy and the violent rain event were on consecutive days (27. and 28.05.2017). From May until July 2017 the precipitation rate ranged between 0 and 55 mm d⁻¹ and averaged at 9.77 mm d⁻¹.

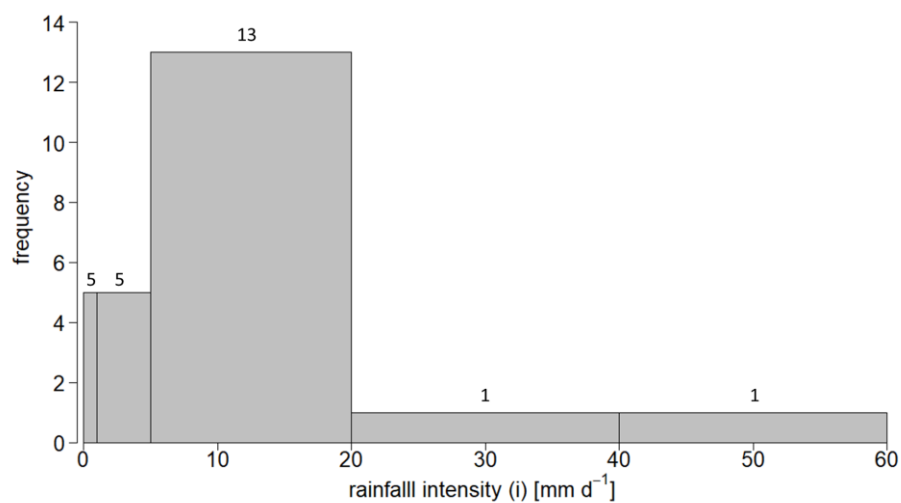


Figure 8 Frequency distribution of rainfall intensity based on daily intensities during the time period of sample collection.

The concentrations of DOC, I, Fe and Br in precipitation were 3.6 mg L⁻¹, 1.4 µg L⁻¹, 1.8 µg L⁻¹ and 5.0 µg L⁻¹ respectively (Tab. 4).

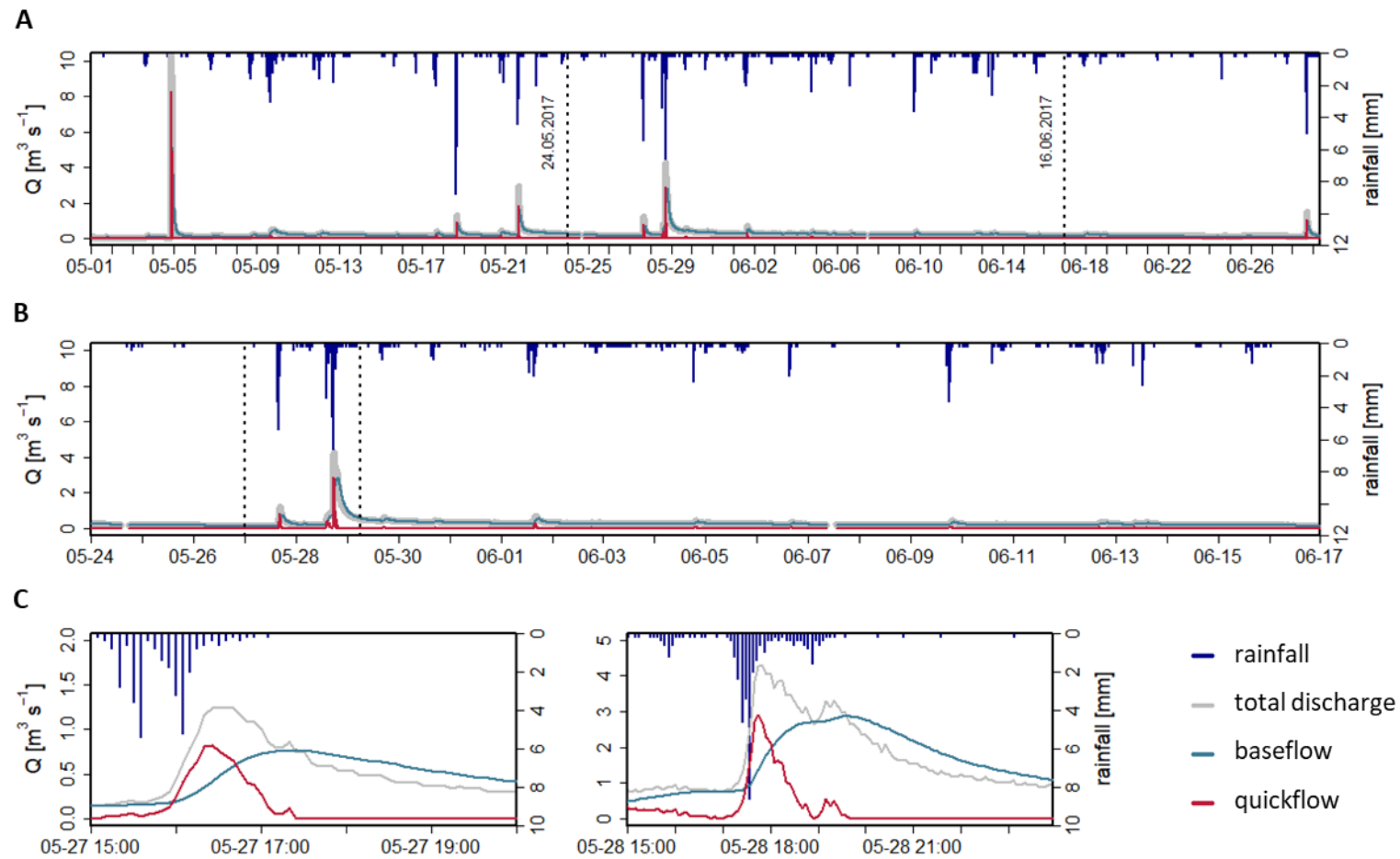


Figure 9 Hydrograph: 5 min interval precipitation, total discharge with time series of runoff separated into baseflow and quickflow components during A) 05.01-30.06; B) 24.05-16.06 (examination time) and C) during event 1: 27.05 (left) and 2: 28.05 (right). Here the automatic measurements are depicted. Precipitation: blue bars, total discharge: grey line, baseflow: blue line, quickflow: red line.

3.2.2 Streamflow discharge

The annual amount of streamflow in 2017 was 3766 mm (Birkel 2017). The discharge varied between 0.14 and 4.27 m³ s⁻¹, consistent with the variations in precipitation as illustrated by the hydrograph shown in Figure 9.

Heavy precipitation events, especially on the 27.05.17 (event 1) and 28.05.2017 (event 2) leading to a visible delayed response in discharge increase after around 50 minutes during event 1 and 20 minutes during event 2 meaning that rainwater reaches the river with a delay of that lag time (delay between peak rainfall and peak discharge). The stormflow hydrograph is characterized by a rapid rise and slower recession (Fig. 9).

3.2.3 Separation of baseflow and quickflow

The applied RDF-method (see 2.4.3) to separate the streamflow of Q_M into baseflow and quickflow revealed baseflow as the dominant component of the streamflow during measuring time. During single precipitation events total discharge was composed entirely of baseflow. Only during event 1 and 2 the quickflow exceeded the baseflow of Q_M . During this time just one grab sample was taken in Q_M , Q_L , and Q_R , respectively. Baseflow increased shortly after the rising limb of the total stream discharge and peaked after maximum discharge. Quickflow peaked at the same time with the total discharge (Fig. 9, Tab. 3). On average, discharge increased from 0.20 m³ s⁻¹ under baseflow conditions to 0.53 m³ s⁻¹ under quickflow conditions (Tab. 4).

Table 3 Time of peak rain intensity or discharge sorted by water type. P: precipitation; Q_M : total discharge; BQ: baseflow; DQ: quickflow: Here the automatic measurements are depicted

	05-27 [hh:mm]	05-28 [hh:mm]	06-01 [hh:mm]	06-04 [hh:mm]
P	15:35	17:25	15:20	18:30
Q_M	16:25	17:45	16:00	18:55
DQ	16:25	17:45	16:00	18:55
BQ	17:25	19:35	17:15	19:55

Overland flow occasionally occurred after long and intense precipitation mainly on non-protected areas like trails but was not sampled.

3.2.4 Stream water chemistry during baseflow and quickflow

The average of physical parameters and element concentrations in stream water of Q_M were calculated during periods with and without quickflow to indicate the influence of surface runoff in chemical composition of the discharge (Tab. 4).

In Q_M , almost all element concentrations were increased during quickflow conditions compared to baseflow conditions (Fig. 10).

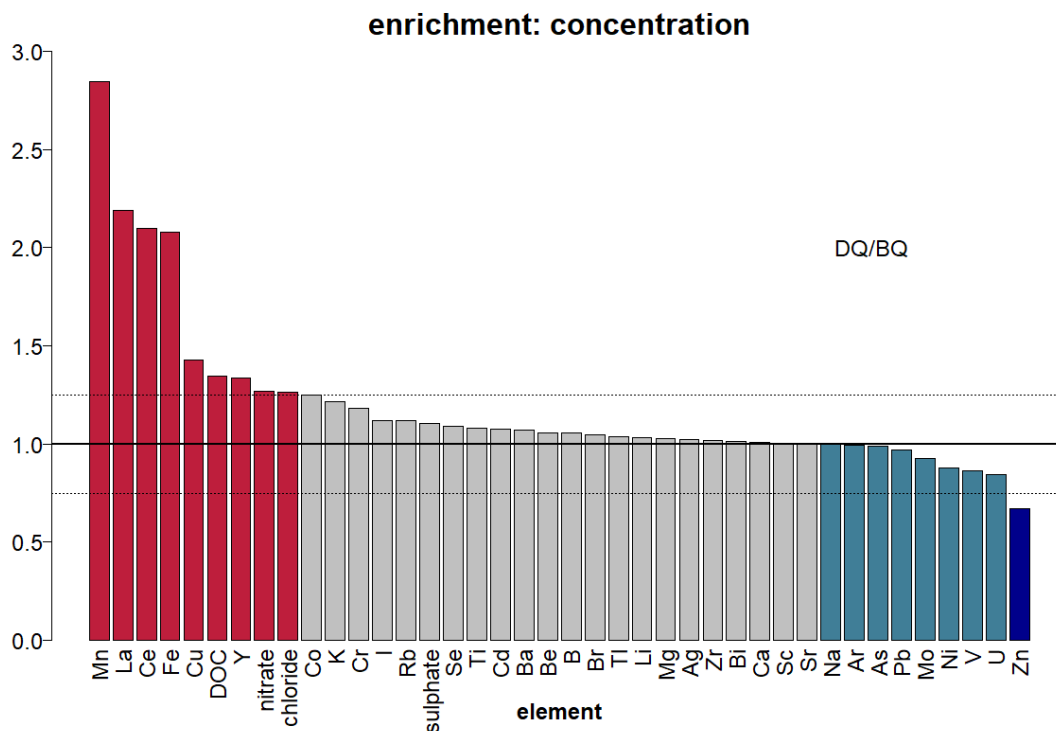


Figure 10 Enrichment factors for all element concentrations during quickflow conditions against baseflow conditions in Q_M , sorted from highest to lowest. Enrichment factor of >1.25 : red bars, enrichment factors between 1.25 and 1: grey bars, depletion factors between 1 and 0.75: light blue bars, depletion factor of <0.75 : dark blue bars. Boundary between enrichment and depletion (enrichment factor of 1): black solid line.

The highest increase in concentration was measured for Mn (enrichment factor >2.5), followed by La, Ce, Fe, Cu, DOC, Y, NO_3^- and Cl^- (enrichment factor >1.25). For example, K, SO_4^{2-} , Mg and Ca slightly increased (enrichment factor between 1.25 and 1) and Na, V, U (enrichment factors <1) and Zn (enrichment factor <0.75) decreased. I enrichment factor was 1.12 (Fig.10). Rain water exhibited higher I, DOC and Fe and lower Br concentrations than stream water under both, base- and quickflow conditions. Therefore, compared to rain, changes in concentrations between base- and quickflow were low (Tab. 4).

Average DOC concentrations in runoff ranged from 0.9 mg L^{-1} under baseflow conditions to 1.3 mg L^{-1} (34.5 % increase) during quickflow events. Fe concentration increased by 108 % from 0.4 to $0.9 \text{ } \mu\text{g L}^{-1}$. The increase of *I* concentration was just 12.2 %, from 1.0 to $1.1 \text{ } \mu\text{g L}^{-1}$. Br concentration increased by 4.5 % from 6.6 to $6.9 \text{ } \mu\text{g L}^{-1}$ (Tab. 4). An increase in discharge was accompanied by a decrease in pH during heavy rain events. The median of pH decreased from 6.9 under baseflow to 6.7 under quickflow conditions in Q_M . The EC was nearly the same in stream water during quickflow and baseflow but slightly higher in stream water under baseflow conditions (Tab. 4).

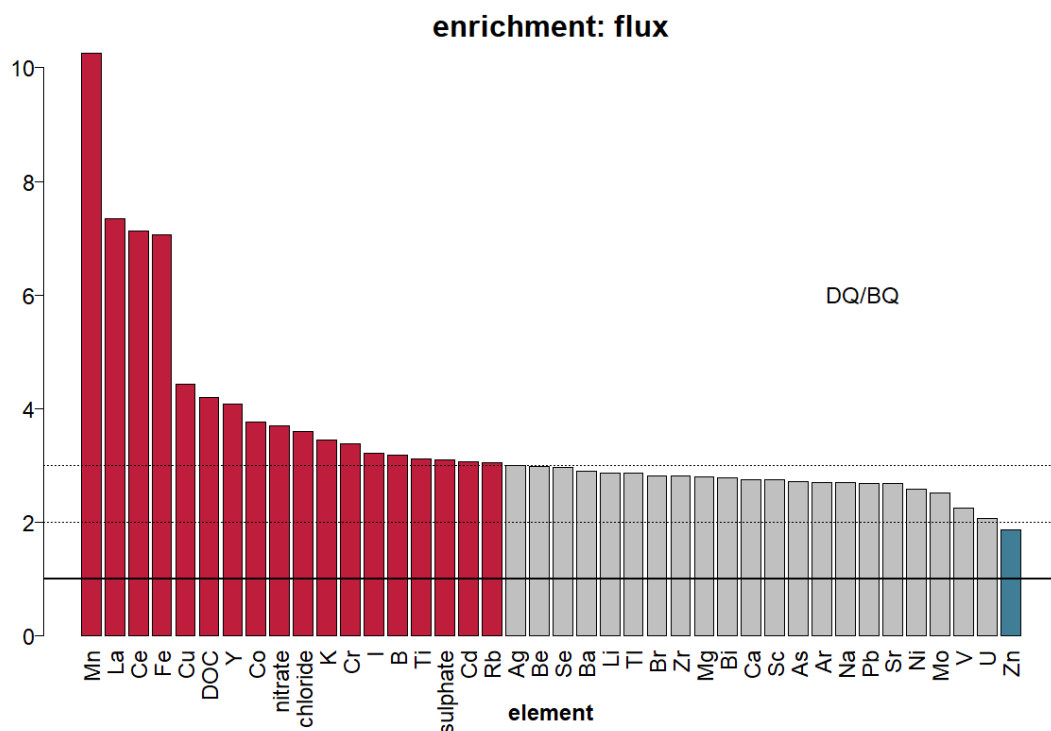


Figure 11 Enrichment factors for all element fluxes during quickflow conditions against baseflow conditions sorted from highest to lowest. Enrichment factor of >3 : red bars, enrichment factors between 3 and 2: grey bars, enrichment factors between 2 and 1: light blue bars. Boundary between enrichment and depletion (enrichment factor of 1): black solid line.

All fluxes increased during quickflow conditions (Fig. 11). The *I* enrichment factor was 3.22.

3 Results

Table 4 Mean concentrations (Ca, Mg, K, Na, Cl; DOC, I, Br, Fe) of chemical constituents, discharge (Q), pH and conductivity (EC), redox potential (Eh) sorted by water type. P: precipitation; Q: total stream water in Q_M (all samples); BQ: stream water during baseflow; DQ: stream water during quickflow

Type	No. Samples		Q [$m^3 s^{-1}$]	pH	EC [$\mu S cm^{-1}$]	Eh [mV]	DOC [$mg L^{-1}$]	I [$\mu g L^{-1}$]	Br [$\mu g L^{-1}$]	Fe [$\mu g L^{-1}$]	Ca [$mg L^{-1}$]	Mg [$mg L^{-1}$]	K [$mg L^{-1}$]	Na [$mg L^{-1}$]	Cl [$mg L^{-1}$]
P	1		-	-	-	-	3.55	1.42	4.98	1.83	1.33	0.34	2.03	0.38	
Q	14	Mean	0.27	6.84	27.22	386	1.02	0.98	6.68	0.54	2.27	0.73	0.79	1.80	1.75
		STD	0.69	0.03	0.02	0.05	0.44	0.08	0.05	0.79	0.03	0.04	0.12	0.06	0.13
		Min	0.14	6.50	26.00	355	0.54	0.90	6.03	0.13	2.18	0.65	0.63	1.52	1.45
		Max	0.87	7.05	28.00	414	1.91	1.26	7.26	1.81	2.41	0.78	1.00	1.96	2.36
		Median	0.20	6.92	27.00	380	0.85	0.97	6.63	0.42	0.01	0.74	0.79	1.81	1.68
BQ	11	Mean	0.19	6.88	27.29	390	0.95	0.96	6.62	0.44	2.27	0.73	0.76	1.80	1.65
		STD	0.24	0.03	0.02	0.05	0.42	0.03	0.05	0.61	0.03	0.05	0.08	0.06	0.06
		Min	0.14	6.50	27.00	371	0.54	0.90	6.03	0.13	2.18	0.65	0.63	1.52	1.45
		Max	0.30	7.05	28.00	414	1.73	1.01	7.23	0.96	2.41	0.78	0.84	1.96	1.83
		Median	0.18	6.93	27.00	380	0.74	0.96	6.62	0.28	2.26	0.73	0.78	1.83	1.65
DQ	3	Mean	0.53	6.69	27.00	373	1.27	1.07	6.92	0.91	2.29	0.75	0.92	1.80	2.09
		STD	0.47	0.03	0.04	0.05	0.41	0.12	0.04	0.70	0.02	0.01	0.07	0.02	0.13
		Min	0.27	6.54	26.00	355	0.62	0.97	6.52	0.40	2.25	0.74	0.86	1.76	1.73
		Max	0.87	7.00	28.00	390	1.91	1.26	7.26	1.81	2.35	0.76	1.00	1.84	2.36
		Median	0.44	6.54	27.00	373	1.28	0.99	6.97	0.52	2.27	0.75	0.91	1.79	2.17

Table 5 Spearman correlation coefficients of the total discharge of Q_M (Q), baseflow (BQ), quickflow (DQ), turbidity, pH, rain and element concentrations. Non-significant correlations are marked in grey

	Q	BQ	DQ	Turbidity (50)	Turbidity (2000)	pH	rain	DOC	I	Fe
Q	1	0.87***	0.68**	0.63*	0.67**	-0.20	0.53	0.53	0.46	0.52
BQ	0.87***	1	0.37	0.46	0.50	-0.32	0.21	0.48	0.44	0.48
DQ	0.68**	0.37	1	0.71**	0.68**	-0.12	0.67**	0.28	0.48	0.38
pH	-0.20	-0.32	-0.12	-0.33	-0.38	1	0.20	-0.03	0.06	-0.11
rain	0.53	0.21	0.67**	0.55*	0.55*	0.20	1	0.37	0.31	0.40
DOC	0.53	0.48	0.28	0.15	0.17	-0.03	0.37	1	-0.06	0.45
Cl	0.72**	0.56*	0.64*	0.80**	0.83***	-0.56*	0.55*	0.46	0.06	0.53
Br	0.62*	0.73**	0.31	0.52	0.54	-0.59	0.09	0.28	-0.02	0.570*
I	0.46	0.44	0.48	0.41	0.40	0.06	0.31	-0.06	1.00	0.19
Fe	0.52	0.48	0.38	0.39	0.42	-0.11	0.40	0.45	0.19	1
Ca	-0.38	-0.60*	0.13	-0.05	-0.09	0.11	0.38	-0.35	-0.14	-0.11
K	0.34	0.14	0.71**	0.27	0.24	-0.26	0.31	0.22	0.42	-0.02
Na	-0.32	-0.35	-0.12	-0.40	-0.41	0.07	0.10	-0.14	-0.43	0.09

P < 0.05, **P < 0.01, ***P < 0.001

3.3 Comparison of the streams: Q_M , Q_L and Q_R

To ensure comparability between the three streams (Q_M , Q_L and Q_R), only manual measurements (discharge, pH, redox potential, Tds, conductivity) and manual samples of Q_M are used in further calculations (correlations, means), unless otherwise stated.

3.3.1 Physical parameter

The discharge measured manually ranged between 0.14 and 0.93 $\text{m}^3 \text{s}^{-1}$ (Fig. 12) for Q_M , between 0.00088 and 0.0096 $\text{m}^3 \text{s}^{-1}$ for Q_L and between 0.012 and 0.031 $\text{m}^3 \text{s}^{-1}$ for Q_R . The average discharge for Q_M was 0.27 $\text{m}^3 \text{s}^{-1}$, 0.006 $\text{m}^3 \text{s}^{-1}$ for Q_L and 0.02 $\text{m}^3 \text{s}^{-1}$ for Q_R . Q_L is the tributary with the lowest discharge (27.97 percent of Q_R and 2.19 percent of Q_M).

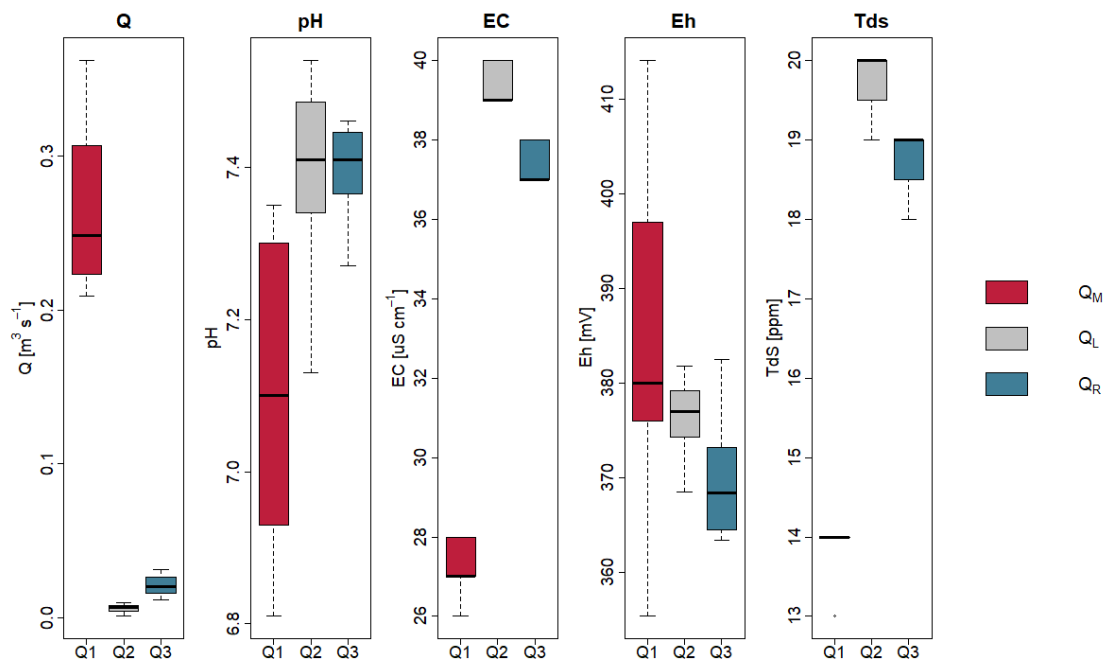


Figure 12 Boxplots of physical parameters (Q , pH , EC , Eh , Tds) in the main channel Q_M and the two tributaries Q_L and Q_R . Q_M : red bar, Q_L : grey bar, Q_R : blue bar.

The pH ranged between 6.8 and 7.4 for Q_M , between 7.1 and 7.5 for Q_L and between 7.3 and 7.5 for Q_R . On average, the pH was 7.1 for Q_M and 7.4 for Q_L and Q_R .

EC , pH as well as Tds were higher in Q_L and Q_R (average: Q_L : $39.4 \mu\text{S} \cdot \text{cm}^{-1}$, 19.8 ppm; Q_R : $37.4 \mu\text{S} \cdot \text{cm}^{-1}$, 18.7 ppm) than in Q_M (average: $27.22 \mu\text{S} \cdot \text{cm}^{-1}$, 13.8 ppm). Eh was lower in Q_R (average: 370 mV) and Q_L (average: 376 mV) and the highest in Q_M (average: 386 mV).

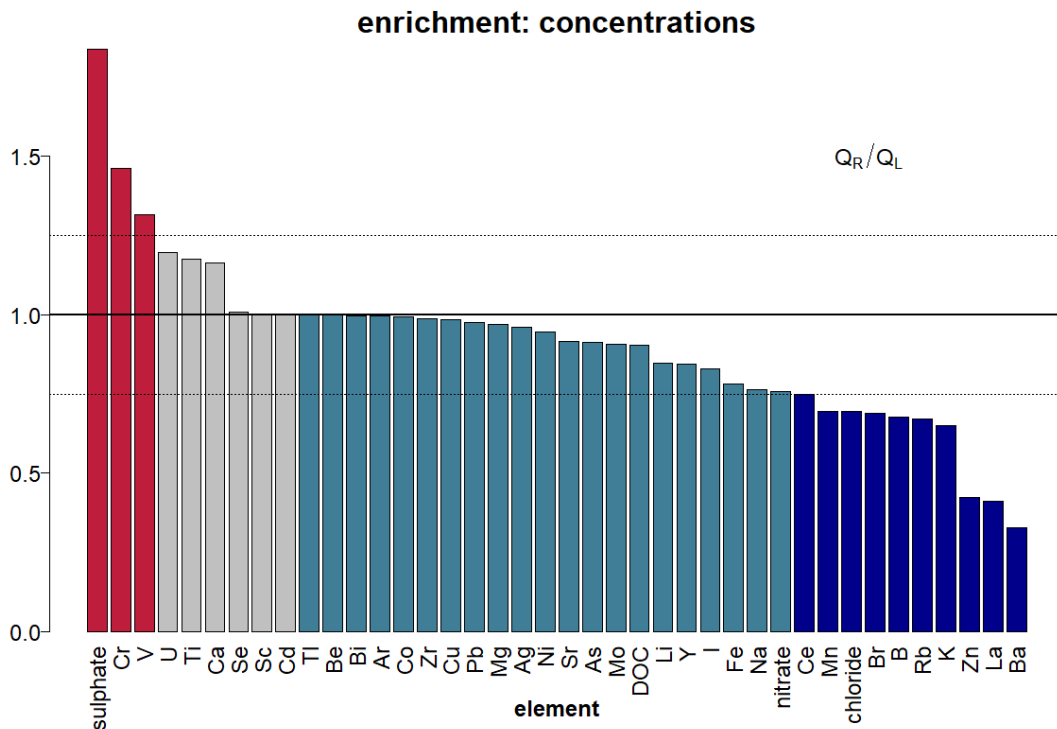
3.3.2 Stream water chemistry of Q_M, Q_L, and Q_R

Figure 13 Enrichment factors for all element concentrations in stream water of Q_R against Q_L sorted from highest to lowest. Enrichment factor of >1.25: red bars, enrichment factors between 1.25 and 1: grey bars, depletion factors between 1 and 0.75: light blue bars, depletion factor of <0.75: dark blue bars. Boundary between enrichment and depletion (enrichment factor of 1): black solid line.

The most element concentrations were higher in C_L than in C_R, including Zr, Mg, DOC, Al, I, Fe, Na, Cl and K (Fig. 13). SO₄²⁻, Cr, V, U, Ti, Ca, Zn concentrations were higher in Q_R.

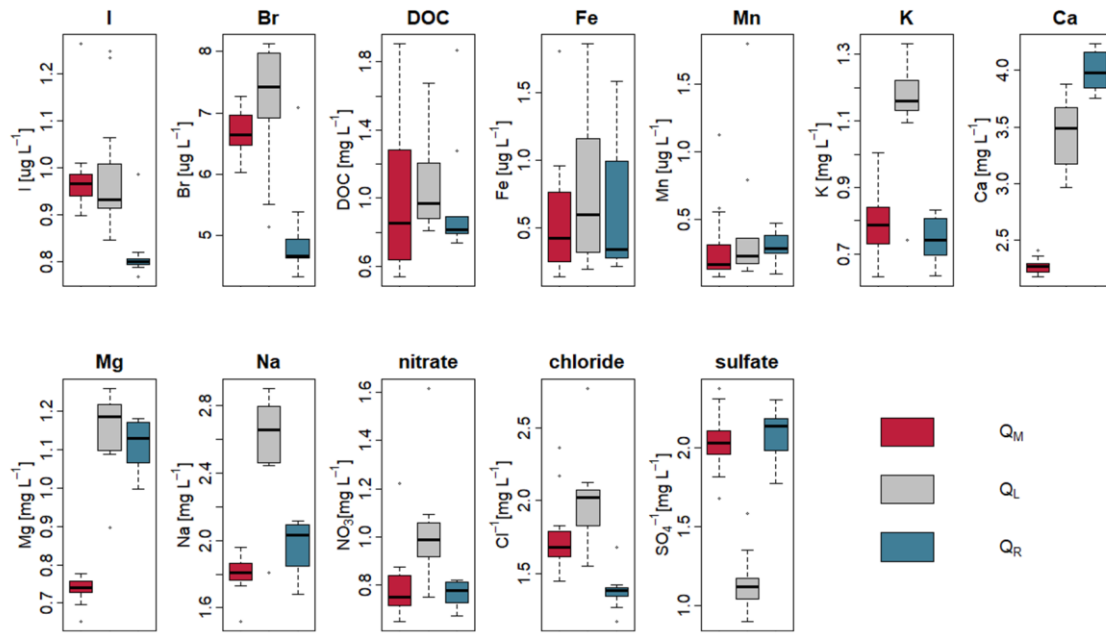


Figure 14 Boxplots of element concentrations during sampling period in the main channel Q_M and the two tributaries Q_L and Q_R Manually taken samples only. Q_M : red bar, Q_L : grey bar, Q_R : blue bar.

On average, DOC concentration in all streams was 1 mg L^{-1} , I concentration was between 0.8 and 1 µg L^{-1} and Fe concentration was between 0.5 and 0.8 µg L^{-1} . A high variability in DOC and Fe concentrations for each stream could be observed (Fig. 14).

3.3.3 Element fluxes of Q_M, Q_L, and Q_R

In comparison, the mean flux of elements of Q_L was lower than that of Q_M and Q_R (Fig. 15). Only the flux of Ba was higher in Q_L than in Q_R

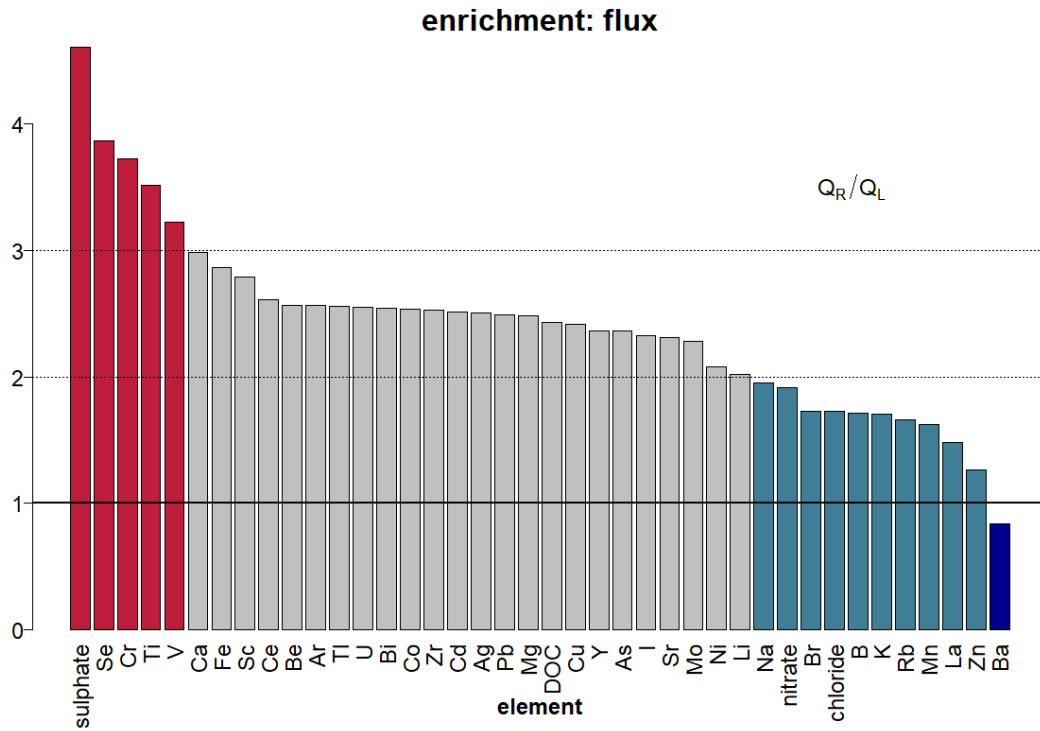


Figure 15 Enrichment factors for all element fluxes of Q_R against Q_L sorted from highest to lowest. Enrichment factor of >3: red bars, enrichment factors between 3 and 2: grey bars, enrichment factors between 2 and 1: light blue bars, depletion factor of <1: dark blue bars. Boundary between enrichment and depletion (enrichment factor of 1): black solid line.

3.4 Element content in biofilm samples

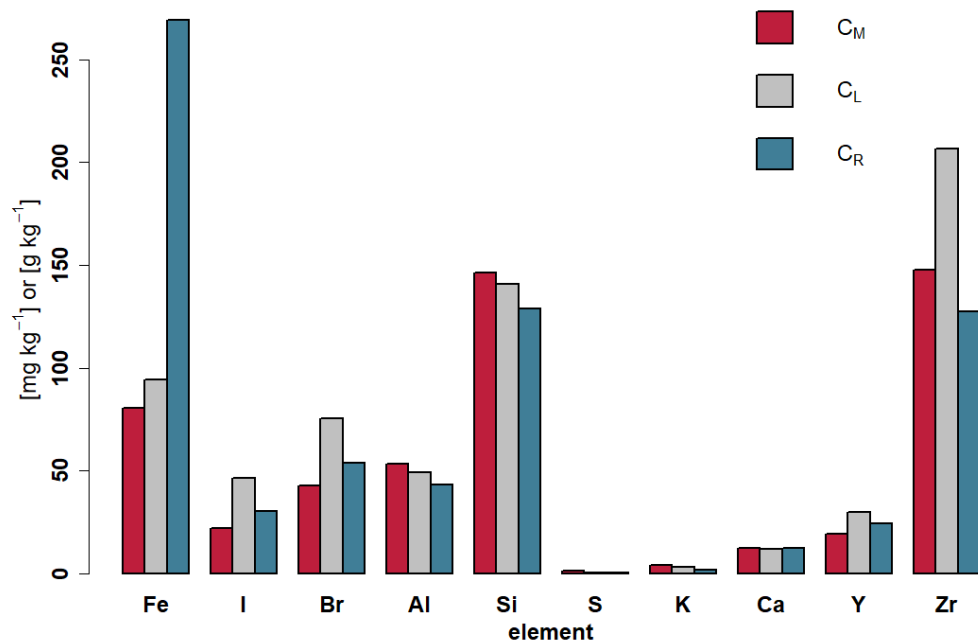


Figure 16 Concentration of elements in biofilms of Q_M (red), Q_L (grey) and Q_R (blue). I , Br , Y , Zr [$mg\ kg^{-1}$] and Fe , Al , Si , S , K , Ca [$g\ kg^{-1}$].

To investigate the fate of I in river systems, I was measured in biofilms. The concentration of I in the biofilm samples was the highest in Q_L and the lowest in Q_M . I comprised $22.2\ mg\ kg^{-1}$ in Q_M , $46.6\ mg\ kg^{-1}$ in Q_L and $30.4\ mg\ kg^{-1}$ in Q_R . Fe concentration was the lowest in Q_M , but the highest in Q_R . (Fig. 16). Br , Al , Si , K , Y and Zr were higher in Q_L than in Q_R .

3.5 Parent rock analysis

Andesite (A) and volcanic conglomerate (Vc) revealed the following element concentrations (Tab. 6).

Table 6 Concentrations of chemical constituents, sorted by parent rock type. Andesite (A) and volcanic conglomerate (Vc)

Type	I	Fe	Zr	Br	Cu	K	Ca	Mn
	[$mg\ kg^{-1}$]	[$g\ kg^{-1}$]	[$mg\ kg^{-1}$]	[$mg\ kg^{-1}$]	[$mg\ kg^{-1}$]	[$g\ kg^{-1}$]	[$g\ kg^{-1}$]	[$g\ kg^{-1}$]
A	0.72	79.03	65.95	1.78	108.72	2.4	64.0	1.44
Vc	1.23	74.37	80.73	4.02	130.57	1.47	11.8	0.72

3.6 Iodine enrichment compared to bromine

The comparison between I:Br-ratios in stream water, leachates, biofilms, parent rocks and throughfall offers estimates regarding differences in I and Br biogeochemistry. An I:Br-ratio lower than one indicates higher Br than I concentrations, a ratio higher than one indicates higher I concentrations in the sample in relation to Br.

Table 7 Mean iodine : bromine (I:Br)-ratios in stream water during the entire examination time (Q), baseflow (BQ) and quickflow (DQ) conditions, in leachates, biofilms and parent rocks (Andesite (A) and volcanic conglomerate (Vc))

Type	F1 [mg kg ⁻¹]	F2 [mg kg ⁻¹]	F3 [mg kg ⁻¹]	F4 [mg kg ⁻¹]	F5 [mg kg ⁻¹]
I:Br	0.36	0.55	0.43	2.59	0.46

Type	Q [μg L ⁻¹]	BQ [μg L ⁻¹]	DQ [μg L ⁻¹]	Biofilm [mg kg ⁻¹]	throughfall [μg L ⁻¹]	A [mg kg ⁻¹]	Vc [mg kg ⁻¹]
I:Br	0.15	0.15	0.16	0.52	0.29	0.40	0.31

The I:Br-ratio in the throughfall (0.29) was higher than the mean ratio in the stream water during baseflow (0.15) and quickflow (0.16) conditions, respectively, but lower than the mean ratio of the leachates of F1 (0.36) (Tab. 7).

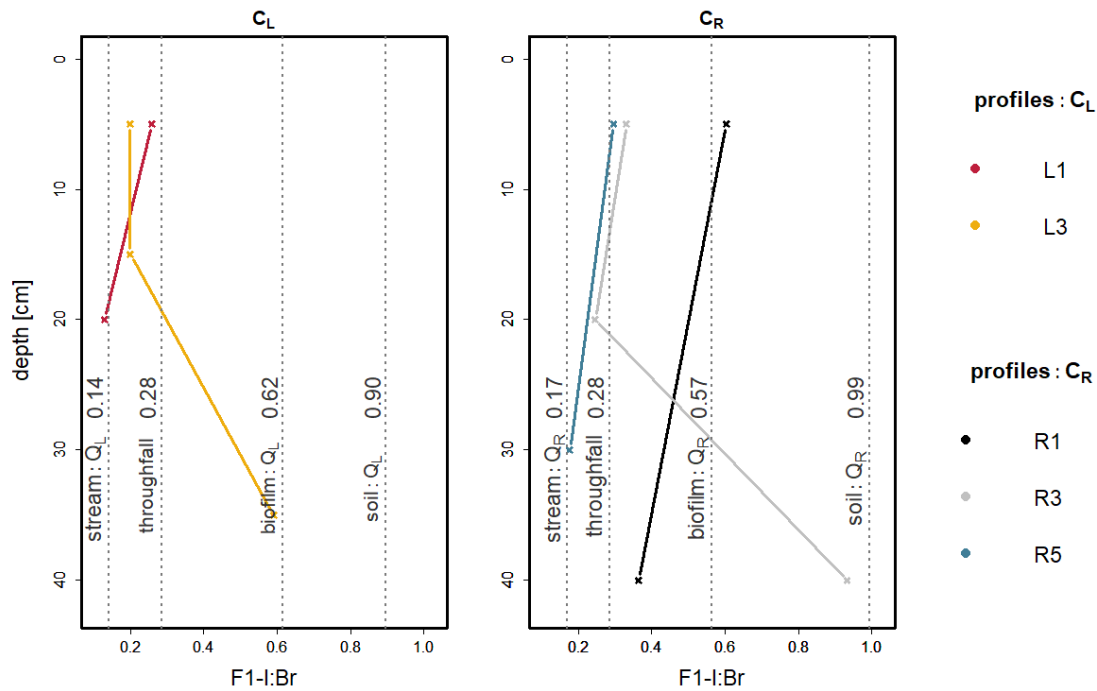


Figure 17 Extractable iodine concentrations [mg kg^{-1}] divided by extractable bromine concentrations of F1 in profiles L1 (red), L3 (dark yellow), R1 (black), R3 (grey), R5 (blue). Iodine-bromine-ratios in the respective stream water, biofilm, solid soil samples (measured by Schulz (2018)) and throughfall were shown as black dashed vertical lines.

Regarding the vertical I:Br-ratio in the leachates of F1 in soil profiles two patterns were shown. In soil profiles sampled at three depths (L3, R3) the I:Br-ratio first decreased from topsoils to the *I* accumulation horizon and increased in deeper horizons. In L1, R1 and R5 the I:Br-ratio decreased with soil depth. In all soil profiles the I:Br-ratio in the topsoil horizon was near and mostly lower the I:Br-ratio found in the throughfall, except for R1 with a higher I:Br-ratio (Fig. 17). The I:Br-ratios of the extraction steps F2, F3 and F4 are shown in the appendix (Fig. 22-24).

In contrast to the I:Br-ratios found in the leachates of F1, F2, F3 and F5, the ratio in the F4-leachate was higher than 1 (2.59).

4 Discussion

Results show, that despite the high *I* concentration in solid soil (median: 69 mg kg⁻¹, range: 52.7-129.6 mg kg⁻¹ (Schulz 2018)), *I* concentration in stream water was rather low ranging between 0.77-1.26 µg L⁻¹ during base- and even stormflow conditions. These findings are different from those found in temperate catchment systems where concentrations in soils are by a factor of 13 lower (referred to the mean *I* concentration in soils reported by Johnson (2003)). But *I* concentrations in rivers and lakes are comparable to the values found by Gilfedder et al. (2010) in Germany (range: <1-10 µg L⁻¹). This indicates a strong sorption of *I* to the soil matrix. Solid phase sequential extraction identified *I* sorption to metal-oxides as the main retention factor (median: 79 % of total *I*) and negligible *I* mobility (median: 0.2 % of total *I*).

4.1 Iodine enrichment and sorption in soils

I concentrations in soils are dependent on the soil type with a worldwide range from <0.1 to 10 mg kg⁻¹ (Moreda-Piñeiro et al. 2011). Johnson (2003) reported that the mean *I* concentration in soils is 5 mg kg⁻¹; the highest determined amount was 150 mg kg⁻¹. Higher soil *I* contents were just observed in coastal areas for example with a concentration up to 660 mg kg⁻¹ in Northern Ireland in an organic-rich soil (Smyth and Johnson 2011). In Japanese andosols, *I* concentrations between 0.2 and 150 mg kg⁻¹ were, according to the authors, caused by marine influence, high rainfalls (2000 mm yr⁻¹) and high adsorption capacities (Muramatsu et al. 2004). Hence, in comparison to other studies, determined *I* concentration in the soils (analysed by Schulz (2018)) of this study are in the higher range (median: 69 mg kg⁻¹). *I* enrichment during the weathering process can be supposed to be neglectable because *I* contents in parent rocks are much lower (< 1 mg kg⁻¹) than in overlaying soils in the ReBAMB (Whitehead 1984). In accordance with previous studies (Johnson 2003; Smyth and Johnson 2011; Whitehead 1984) the high *I* accumulation may be attributable to high deposition/precipitation rates, high retention of *I* in the soil and consequently low mobilization and volatilization rates (Muramatsu et al. 2004). In comparison to the global mean concentration of *I* in rainwater (0.5-5.0 µg L⁻¹) atmospheric inputs to the studied soils are in the lower range (1.42 µg L⁻¹). But the high rainfall with total annual precipitation of around 3589 mm leads to high annual *I* depositions to the soils in the ReBAMB. Due to the high soil age compared to soils developed after the last ice age, tropical soils had a long time for *I* accumulation and storage. The loss of *I* from soils is difficult to quantify and may occur via leaching, volatilization, and removal in crops (Whitehead 1984).

4.1.1 Solid phase iodine binding

According to the results of the solid phase sequential extraction experiments, *I* is mainly sorbed to reducible components in the soil. This includes iron sesquioxides (Fe_2O_3), hydroxides ($\text{Fe}(\text{OH})_3$) and oxide hydroxides ($\text{FeO}(\text{OH})$).

Fe-oxides were found as the main soil component for *I* retention in acidic soils and sediments (Li et al. 2013; Whitehead 1973, 1974). The sequential extraction of sediments by Li et al. (2013) revealed high sorption of *I* to Fe-oxyhydroxides and secondarily to OM. Positive correlation between *I* and sesquioxide content was also documented in 23 soils in England (Whitehead 1973).

The low pH (range: 4.5-5.5 (Schulz 2018)) in the catchments soils favours *I* retention by metal-oxides (Couture and Seitz 1983; Hu et al. 2005; Hu et al. 2009; Shetaya et al. 2012; Yoshida et al. 1992). Particularly Fe-oxides appear to be increasingly important under more acidic conditions (Whitehead 1978), as a result of the point of zero charge (6-8) (Kaplan 2003) which is higher than the actual pH in the soils of the ReBAMB.

The soils in the ReBAMB are characterized by high carbon (C) contents (median: 62 g kg^{-1}) (Schulz 2018). Due to the high affinity of *I* to bind to OM, it might have been expected that the sequential extraction showed higher portions of Org-*I*, as other studies showed SOM as the main factor controlling *I* sorption in soils (Dai et al. 2009; Hu et al. 2009; Schwehr et al. 2009; Shetaya et al. 2012; Shimamoto et al. 2011; Zhang et al. 2011). Further, K_d values of Org-*I* are greater than that of inorganic *I* (Hu et al. 2012; Schwehr et al. 2009). Schulz (2018) found lower *I* values in solid samples in topsoil horizons than in the horizons below (except for profiles L4 and R4, which were not used in this thesis). Thus, in most of the soil profiles an *I* accumulation horizon (L1: 20 cm, L3: 15 cm, R1: 40 cm, R3: 20 cm, R5: 30 cm) with higher *I* values than in topsoil horizons (5 cm) was found (Fig. 7). Further, a weak correlation ($r_s = 0.42$, $p < 0.05$) between *I* and C in the solid samples was determined (Schulz 2018).

The indirect determination of *I* bound to OM [F5-*I*] revealed higher values in topsoils and a decline in Org-*I* with soil depth (except for R3). I-metal-complexes [F4-*I*] have the highest concentrations either in the accumulation horizons of total *I* (in soils sampled in three different depth; L3, R3) or showed an increase in *I* concentration with soil depth (L1, R1, R5). The percentage of I-metal-complexes [F4-*I*%] increased with soil depth (except for R3). In contrast, the percentage of organically bound *I* [F5-*I*%] decreased with soil depth (except for R3). It can be assumed that the formation of Org-*I* is more important in upper horizons. The deeper in the

soil, the role of OM decreases with an increasing role of metal-oxides at the same time. Because the amount of *I* bound to metal-oxides and the total amount of *I* in soil horizons decreased under the *I* accumulation horizon (Schulz 2018), just small amounts of *I* reach underlying soil horizons in spite of the increasing role of metal-oxides in *I* retention with increasing depth (Fig. 7).

Despite the high degree of *I* bound to metal-oxides surfaces (median: 79 % of total *I*), revealed by the sequential extraction, it is likely that during F4 also *I* sorb to metal-oxides through the presence of OM (Li et al. 2013) or vice versa (Qian et al. 2017) was extracted. Qian et al. (2017) stated that Fe fulfils a bridging function in the formation of binary and ternary complexes with OM.

In addition, the formation of Org-*I* species is enhanced by microorganisms and/ or enzymes, especially the reaction with high molecular weight OM. In this study, the soil was organic rich and high in microbial activity. This would favour the transformation of inorganic *I* to Org-*I* species mediated by bacterial enzymes (Zhang et al. 2011) and would support the assumption that *I* is bound to Fe-oxides through OM/DOM sorption. Thus, it is assumed that the degree of *I* bound to OM is underestimated by the conducted sequential extraction, because dissolution of Fe-oxides in F4 will mainly release Org-*I* bound to Fe-oxides.

The sequential extraction procedure includes further uncertainties arising from re-adsorption to the residue of the extraction step, cross-contamination, incomplete digestion, release of other *I* forms, volatilization or transformation of *I*, especially in a strong acid/base solution (Hou et al. 2009; Shimamoto et al. 2011).

4.1.2 Water soluble iodine in soils

There are two different *I* mobility patterns in the soils of the ReBAMB. In L1, R1 and R5, *I* mobility was the highest in topsoil horizons (5 cm) and declined with increasing depth (L1: 20 cm, R1: 40 cm, R5: 30 cm). In L3 and R3, *I* mobility was the lowest in the *I* accumulation horizon (15-20 cm) and was higher in upper (5 cm) and lower soil horizons (>20 cm). Thus, in the soil profiles the *I* mobility was the lowest in the respective *I* accumulation horizon (L1: 20 cm, L3: 15 cm, R1: 40 cm, R3: 20 cm, R5: 30 cm). In contrast, Schulz (2018) found a decline in *I* mobility with increasing depth in all soil profiles of the ReBAMB with the highest mobility in topsoils and a correlation between *I* and DOC water leachability ($r_s = 0.7$, $p < 0.001$). Nevertheless, it can be concluded that *I* water-solubility (mean: 0.2 %) was low despite high *I* contents in the soil and showed higher mobility in topsoil horizons in most of the profiles than in the underlying soil horizons.

The strong sorption of *I* or Org-*I* under the low pH conditions in the investigated soils explains low *I* leaching with water (F1). The low degree of cold water soluble *I* was shown in previous studies (Johnson 2003). The lowest dissolution of *I* was found between a pH of 4.0-5.5 and a temperature between 5-30 °C in forestlands and upland fields of Japan (Yuita et al. 1991). The temperature (21 °C) and pH in the ReBAMB was in that low dissolution range of *I* that favour low *I* transfer into solution.

The C:N-ratio is inversely associated with the degree of OM-decomposition and the water solubility of *I* (F1). Thus, the higher the degree of decomposition of OM, the lower the *I* water solubility. It is assumed that *I* gets incorporated into OM during decay and gets more resistant to biodegradation with decay time like Leri and Myneni (2012) found for Br. Further, it was found that the capacity of OM to sorb *I* increases as decomposition progresses (Whitehead 1974). An increase in Org-*I* concentration with decreasing C:N-ratio was found for example in two peat bogs in southernmost Chile (Biester et al. 2004). Thus, decomposition may enhance *I* stabilization and decrease *I* leachability.

4.1.3 Soil physio-chemical processes: Iodine transport through the soil profile

I distribution with soil depth is widely ranging between soil types (Whitehead 1978). Vertical water movements and interactions between *I* and various soil components (especially SOM, sesquioxides and clay as described above) are crucial for *I* vertical migration in soils (Yoshida et al. 1992) from the surface into the subsoil. Processes such as sorption and (co-) precipitation force *I* retention in the solid phase. Dissolution, complexation and colloid formation force *I* mobilization and migration (Renshaw et al. 2011).

In the soils in the ReBAMB, in most cases the topsoil horizons (5 cm) showed lower *I* concentrations than the horizons below (≥ 15 cm) (Schulz 2018). It is likely that *I* entering the soil via precipitation is primarily fixed by SOM. Due to decomposition of iodinated SOM to DOC (1) (Fig. 18) and infiltrating rain water, small amounts of DOC, *I* and Org-*I* are dissolved into solution. This leads probably to the formation of DOI and thus to co-migration of DOC and *I* as DOI-complexes down the soil profile (2). The mobilization of *I* in small amounts in the uppermost layers is supported by the higher leachable concentrations in water during F1 in topsoil horizons in comparison to deeper soil horizons. It is likely that DOC is the main carrier for *I* in topsoil horizons as Schulz (2018) found a correlation between DOC and *I* ($r_s = 0.7$, $p < 0.001$) and the highest values of DOC in topsoil horizons in water leachates. A small amount of *I* is transported laterally (Yuita et al. 2005) but a considerable amount leached into deeper soil horizons and is retained by metal-oxides. The presence of free metal-oxides leads to sorption of DOI to metal-

oxides and to a lesser extent to direct sorption of *I* to metal-oxides. The amount of free iron oxides is higher in the subsoil horizons than in upper horizons because of weathering and co-translocation of Fe with clay by eluviation-illuviation processes (secondary accumulation) (Maniyunda et al. 2015a). The low mobility of *I* as Org-*I*-Fe-oxide-complex is strengthened by the fact that iron phases protect OM against degradation and stabilize SOM. The degradation rate is decreased compared to unbound OM (Kaiser and Guggenberger 2000; Martínez-Cortizas et al. 2016). Thus, stabilized I-Fe-oxide-OM associations may become enriched over long time, since non-stabilized SOM is degraded more easily. DOC-Fe-oxide-*I*-complexes are likely fixed by clay minerals (4). The correlation between [F4-*I*] and clay ($r_s = 0.57$, $p = 0.051$), further buttressed this relationship. Additionally, the deeper in the soil profile, the finer the texture and the smaller the permeability of the soil. This inhibits fast water flow and thus high *I* mobilization. High Fe contents (median: 114 g kg) and fine texture (Schulz 2018) explain the low *I* solubility and strong fixation in deeper soil horizons. In a podzol investigated by Whitehead (1978) similar *I* accumulation pattern was found in 30-40 cm depth (pH was 3.2). *I* concentration was correlated with the measured Fe concentration (Whitehead 1978).

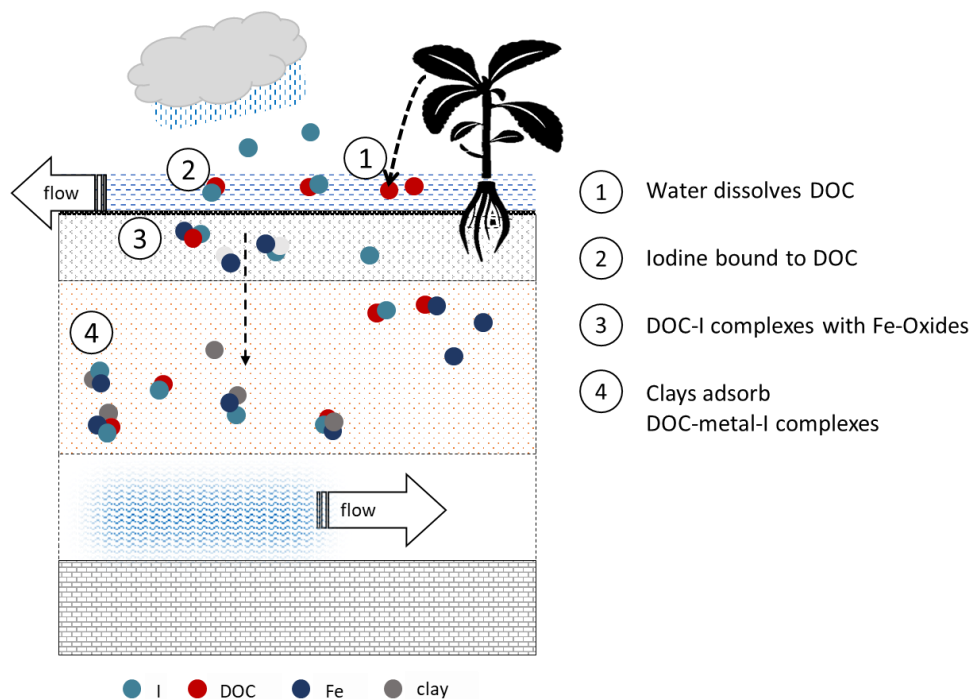


Figure 18 Model of the vertical transport of iodine in soil profiles of the ReBAMB in relationship with organic matter and Fe-oxides.

DOC concentration in leachates measured in the parallel study by Schulz (2018) decreased with soil depth likely because of coprecipitation of Fe and DOC in the upper B horizon (Hope et al. 1994). This process directly influences the DOC concentration in streams (Hope et al. 1994). Further, the low mobility of DOC (median: 0.03 % of total C in the solid soil samples (Schulz 2018)) limits I⁻ leaching from the soils due to the DOC-I⁻ coupling and controls I⁻ concentration in soil water and river water.

In soil profiles sampled at three depths and with an identified I⁻ accumulation horizon, I⁻ mobility increased again with increasing depth. IO₃⁻ has a higher affinity to sorb to soil than I⁻. I⁻ transport is controlled by advection and dispersion and IO₃⁻ is mainly controlled by adsorption. Therefore, it is probably that I⁻ is transferred by water flow to a larger degree than IO₃⁻ and more I⁻ may reach deeper in comparison to IO₃⁻. Sorption of I⁻ is weaker and thus leading to an increase in I⁻ solubility in deeper horizons (Shimamoto et al. 2010). Nevertheless, just very small amounts of I⁻ are transported so deep in the soil because of previous I⁻ incorporation by OM and metal-oxides. Thus, inorganic I⁻ species are only of secondary importance in the soils of the ReBAMB compared to Org-I⁻.

4.1.4 Tropical processes affecting iodine geochemistry

During chemical weathering (oxidation), sesquioxides are formed out of Fe containing primary silicates. Because of high temperatures and precipitation rates the weathering of primary minerals in tropical soils is higher and to a greater depth than in temperate zones. At high microbial activity OM is degraded much faster so that OM remains in the zone near the surface and OM degradation only slightly influence weathering. This leads to the production of more free oxides, especially Fe than in temperate climates because weathering is more complete (neutral or slightly acid hydrolysis and not acid hydrolysis because of acidic organic compounds predominant in temperate soils). The colour of the soils in the studied area was ochreas indicating that more goethite than haematite (more red coloured soils) has been formed during weathering (Duchaufour 1982). Because these soils are on basaltic parent rock, poor in primary silicates, the accumulation of sesquioxides and loss of primary silicates is faster compared to siliceous soils on granite (Zech et al. 2014). This also supports the hypothesis that sesquioxides play an important role in I⁻ retention in the ReBAMB.

A radiotracer batch experiment by Yoshida et al. (1992) found that andosols retain 100 % of added I⁻ and IO₃⁻. The authors stated that IO₃⁻ is sorbed by a specific sorption mechanism similar to the phosphate sorption by free sesquioxides, humus complexes and amorphous silicates (for example allophane), especially in soils with a pH value less than six. These soils showed higher I⁻

retention by oxides than by OM. In soils with a pH higher than six, OM is becoming increasingly important (Yoshida et al. 1992).

A specifically higher IO_3^- sorption affinity for free sesquioxides (Yoshida et al. 1992) would favour inorganic I sorption to sesquioxides in tropical soils. Furthermore, Couture and Seitz (1983) indicated an increase in IO_3^- sorption to Fe-oxides with time due to changes in the reactive surface area (aging) due to slow hydration or abrasion by stirring.

Old weathered acidic tropical soils would thereafter favour I retention by metal-oxides, especially Fe-oxides.

These findings suggest that IO_3^- is present in the soil. However, several previous studies have found DOI as the dominant fraction and low amounts of I^- and IO_3^- in precipitation and aerosols (Gilfedder et al. 2008). The higher input of DOI via atmospheric depositions lead to high amounts of organic species from the beginning of halogen input. Moreover, due to the high affinity of I to sorb to OM, a high proportion of inorganic I in the soil is unlikely.

A high correlation between [F4- I %] and Si content in the soil was found. Si was almost found in all parent materials (Sommer et al. 2006). Si is part of the mineral phase including poorly crystalline (allophane, secondary quartz), amorphous (silica), and crystalline forms (primary silicates, secondary silicates and silicate materials) of Si (Tubana et al. 2016). It is likely that I is bound as organo-metal-complex to clay minerals or allophane leading to the formation of intricate soil complexes. Further studies are needed to investigate the relationship between clay particles and sesquioxides regarding I retention.

Thus, I accumulation in acidic tropical soils is strongly connected with the chemistry of Fe and the related stabilization of OM. Both are controlled by weathering and pedogenic processes and the related high enrichment of I is thus also a result of the high age of tropical soils.

4.2 Influence of catchment hydrology on iodine discharge

Mobilization of I by soil leaching differs in most ecosystems and is affected to a great extent by I sorption in the soil as discussed above and catchment hydrology. Catchment hydrology and runoff composition is driven by the average annual rainfall depth, rainfall regime, antecedent rainfall, topography, physical soil properties, horizon sequence (stratigraphy) (Crespo et al. 2011), catchment size, geology, and land use (Calderon and Uhlenbrook 2016). In tropical steep forested mountain catchments water distribution is controlled mainly by topography and lateral subsurface flow paths in the soil-bedrock interface (Zimmer and McGlynn 2017).

4.2.1 Contributions of quickflow and baseflow to water chemistry

The result of the RDF-method showed that quickflow peaked at the same time as the total discharge, but time between start and end of quickflow was shorter than that of total discharge. Baseflow peaked as the last flow with the longest duration.

The lag time in the catchment (between 20-50 min) was relatively short but longer than the lag time of less than 10 min found by Schellekens et al. (2004). Short lag times are a result of small catchment sizes, steep topographies, short flow path lengths and permeable topsoils with macropores. The catchment described by Schellekens et al. (2004) comprises a smaller size, steeper topography, leading to a comparatively shorter lag time.

Under dry conditions, baseflow is the only flow contributor to streamflow of Q_M based on the RDF-method. Without rainfall, baseflow is composed of groundwater flow through the mineral soil layer discharging into the stream (Broder and Biester 2017; Guzmán et al. 2015) and maintaining flow during dryer periods (Guzmán et al. 2015) (Fig. 19). In contrast, a two-component mixing calculation revealed that during baseflow conditions, the water was composed by $\frac{1}{4}$ out of recent rainfall with a transit time of less than seven days and by $\frac{3}{4}$ out of groundwater (Scholl et al. 2015).

During wet conditions, streamflow can be divided into quickflow and baseflow. The rapid rise and slower recession of the storm hydrograph indicate that there is a source form which water was flowing into the river after the precipitation event stopped. Despite the rapid increase in discharge in Q_M , baseflow is the dominant contributor to stormflow. Quickflow plays just a minor role in streamflow response in Q_M based on the RDF-method. This is in accordance with other tropical catchments (Calderon and Uhlenbrook 2016; Correa et al. 2017; Crespo et al. 2011; Farrick and Branfireun 2015; Scholl et al. 2015).

In addition, past studies found that water discharged into stream during stormflow consisted mostly out of 'old' water (between 75-97 % of total discharge) (Farrick and Branfireun 2015; Pearce et al. 1986; Sklash et al. 1986). 'Old' pre-event soil water stored in near-saturated soil water or groundwater is displaced by 'new' event water from precipitation (current storm water) and is discharged as 'old' water-dominated flow into streams (Farrick and Branfireun 2015). This process is also known as flushing effect (Hope et al. 1994).

The increasing precipitation rapidly delivers water to the stream channel leading to an increase in runoff. Based on the RDF-method storm hydrograph is comprised dominantly of baseflow and to a lesser extent of quickflow.

4.2.2 Separation of streamflow into baseflow and quickflow based on physical parameters

Both water flows are influencing the biogeochemical signature of streams (Renshaw et al. 2011) including element composition, pH, conductivity, redox potential and temperature. Rivers are mostly in the range of neutral pH values, low ionic strength and oxidizing conditions (Renshaw et al. 2011). In the investigated catchment, pH values of Q_M decreased slightly from 6.9 during baseflow conditions to 6.7 during quickflow conditions. This decrease was probably induced by an increase in organic acids input during high precipitation events and related increased surface runoff (Waterloo et al. 2006) draining predominately organic rich topsoil layers.

In comparison, EC remained almost unchanged or slightly decreased in streamflow during stormflow (27.3 to 27 $\mu\text{S cm}^{-1}$). Lower EC in stream water indicates decreasing influence of groundwater (Stewart et al. 2007). A higher EC (between 30 and 102 $\mu\text{S cm}^{-1}$), thus higher solute ionic concentrations, was found by Schellekens et al. (2004) in a small mountainous headwater catchment in northeastern Puerto Rico. Due to the considerable lower EC in Q_M and small changes in EC during base- and quickflow conditions, it can be concluded that the solubility of nutrients and other ions in the ReBAMB is generally low.

4.2.3 Chemical separation of the streamflow

Physical processes and flowpaths in the catchment lead to different concentrations of chemical constituents in the river based on the fluctuating influence of different flow components during base- and quickflow. Thus, due to enrichments or depletions of these chemical constituents the flow generation zones or pathway of the stream water can be determined. Some elements can be divided into groups depending on their major derivation zone in ecosystems. Elements mainly derived from the weathering zone (Na, Ca, Mg) and elements related to vegetation and surface soil horizons (NO_3^- , K, SO_4^{2-}). A change in concentration would indicate changes in water flowpaths in the soil.

K, NO_3^- , SO_4^{2-} are naturally enriched near the soil surface, especially in the litter layer or organic rich horizons (Boucher and Carey 2010; Elsenbeer et al. 1995; Farrick and Branfireun 2015; Schellekens et al. 2004) and are biotically controlled (Scholl et al. 2015). The increase in those element concentrations in stream water of Q_M ($\text{NO}_3^- > \text{K} > \text{SO}_4^{2-}$) resulted from the activation of fast, shallow subsurface pathways through organic rich horizons (like uppermost litter layers) or by surface runoff (Fig. 10). In many tropical catchments a rapid and large increase, particularly

in K, was found during quickflow conditions (Elsenbeer et al. 1995; Farrick and Branfireun 2015; Schellekens et al. 2004).

Na, Ca, Mg in contrast are mainly derived from the weathering zone (Boucher and Carey 2010; Scholl et al. 2015). Thus, an increase in concentration is related to water flow through the weathering zone and therefore groundwater discharge. An increase in precipitation, and thus more water without contact to the weathering zone leads to lower Ca, Na and Mg concentrations in stream water due to dilution (Hessen et al. 2017; Schellekens et al. 2004). In Q_M , Ca, Na and Mg concentrations were nearly the same under quickflow and baseflow conditions (Na slightly diminished under quickflow conditions and Ca and Mg slightly increased). This supports baseflow as the dominant contributor to streamflow in Q_M during rainfall events and an input of precipitation water does not lead to a dilution of baseflow discharge in the streamflow of Q_M because of high infiltration capacities.

The ratio between K and Ca is an indicator of the changing influence of stream water components or pathways (Boucher and Carey 2010). During quickflow conditions an increase in K:Ca-ratio from 0.33 [mg L^{-1}] (0.17 if considering meg L^{-1}) under baseflow conditions to 0.40 [mg L^{-1}] (0.21 meg L^{-1}) was observed. In this case the increase of the ratio identifies rising influence of activated fast, shallow pathways through organic rich horizons. The lower K:Ca-ratio during baseflow conditions indicates water derivation mainly from deeper flow paths and soil horizons of the weathering zone. This fact is supporting the results of the RDF-method and the separation into baseflow and quickflow. In comparison, Schellekens et al. (2004) found an increase from 0.11 under baseflow to 0.19 under stormflow conditions in the K:Ca-ratio in meg L^{-1} indicating higher influence of shallow subsurface or overland flows because of the higher increase.

Shallow lateral subsurface flow or surface pathways dominate during rainfall events in many tropical catchments. However, it is likely that they are not the main contributor to stream runoff in the ReBAMB, because of low changes in K, NO_3^- , SO_4^{2-} , Ca, Na, and Mg concentrations. It can be assumed that vertical flow and the displacement of 'old' or pre-event water are the main factors generating stream runoff during wet and dry periods. However, small differences in the geochemistry and in physical parameters in stream water during baseflow and quickflow indicate an increase of the contributing area of the catchment due to activated shallow subsurface flow paths, even if their influence is low. This also indicates that rainwater has contact to the soil (Fig. 19).

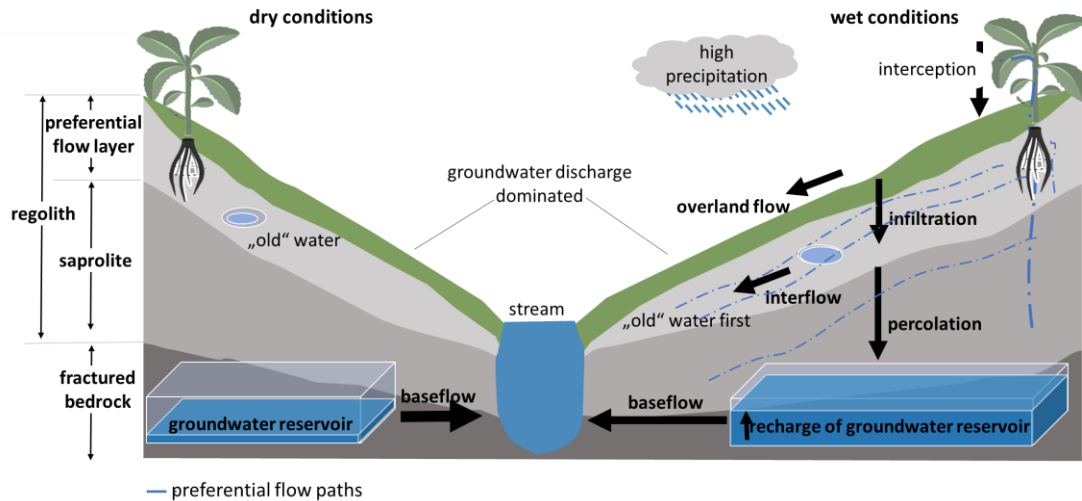


Figure 19 Schematic representation of the hydrologic processes during dry (left side) and during wet conditions (right side) at hillslope scale (adapted from Cheng et al. (2017)).

Examination time was at the beginning of the rainy season which could be another reason why baseflow dominates the hydrograph. Infiltrating rain water percolates deeper and lead to groundwater recharge and thus displacement of stored water after dryer periods. Scholl et al. (2015) found that storm event water was detectable after the events, with exception for one event at the beginning of the rainy season. They concluded that the hydrological dynamics change with proceeding rainy season.

Further, highly weathered soils in tropical climates exhibit mostly deep weathered saprolitic soils so that the boundary between soils and the bedrock can become blurred. This in turn leads to indistinct saturated hydraulic conductivity between weathered and unweathered material making differentiation more difficult (Zimmer and McGlynn 2017) and a separation between different subsurface flows becomes more important the deeper the soil is.

In a study by Correa et al. (2017), an andosol in a small tropical headwater catchment (7.53 km²) in South Ecuador was investigated and soil water contribution to runoff was analysed. The main contributor to runoff and chemical fingerprint in the catchment originated from soil horizons in a depth of 65 cm. They indicated that rainwater infiltrated through the upper porous horizons of the andosol and percolated into deeper horizons (here 0.65 m). The soils were characterized by high porosity, high retention capacities for water and low pH (around 4.8). Similar flows can be assumed in the ReBAMB.

In summary, because of the high loss of rainwater due to interception, high infiltration rates/capacities of the soil and due to the fact that forested catchments reduce overland flow (Calderon and Uhlenbrook 2016) most incoming “new” rainwater is not directly discharged into the stream and causes just a small proportion to total discharge and streamflow response in Q_M . Most of the rainwater is infiltrating through the soil and reaches the groundwater. Thus, flow through the mineral soil layer is responsible for the largest share of discharge variability in the catchment and a baseflow dominated hydrograph.

4.3 Transport of iodine from soils to stream

In Q_M , I concentration increased by 12.2 %, DOC by 34.5 % and Fe by 108 % in stream water under baseflow to quickflow conditions (Tab. 4). An increase was also found by other studies in case of DOC (Broder and Biester 2017; Hope et al. 1994), I (Gutchess et al. 2017) and Fe (Broder and Biester 2017).

It can be assumed that I concentration in groundwater is similar to the concentration during baseflow conditions ($0.95 \mu\text{g L}^{-1}$). The Increase of I concentration during quickflow conditions in stream water was marginal (12 %). Based on this assumption it can be assumed, that during quickflow conditions 88 % of I were derived from groundwater. The remaining 12 % were either transported into stream from the surrounding catchment or were derived by precipitation itself because mobilization was low in the soils in the ReBAMB.

Precipitation falling through the canopy to the soil surface leading to loading with elements (Deb and Shukla 2011) and to I enrichment in throughfall compared to precipitation. In the studied catchment, I ($1.42 \mu\text{g L}^{-1}$) concentration in throughfall was higher than in stream water during baseflow and even quickflow conditions. Since the previous chapter revealed that precipitation that reaches the stream water has contact to the soil, throughfall water enriched in I interacts with the soil, rock and biota. It therefore seems like during water movements through the soil I gets lost from the throughfall water via sorption onto soil surfaces, and interception due to vegetation (Deb and Shukla 2011). I that reaches the soil is bound by SOM, infiltrates as DOI-complex and is fixed by oxides as organic-metal-complex (see chapter 4.1.3). This leads to the assumption that interactions between OM and metal-oxides are affecting the fate of I and that I is mobilized as metal-oxides or OM are mobilized. The results from the sequential leaching test indicate that I associated to metal-oxides can be potentially mobilized under reducing conditions through reductive dissolution of metal-(hydr)oxides because of the redox sensitivity of metal-oxides (Li et al. 2014). However, mobilization caused by reducing conditions is unlikely because

of the high infiltration rates and steep slopes in soils of the ReBAMB and the prevention of backwater.

I incorporated into SOM can be mobilized and released into soil water via microbial degradation of iodinated OM (Anschutz et al. 2000). DOI can infiltrate or can be transported with lateral flow paths into channel water or percolate and recharge groundwater also under oxic conditions. Therefore DOC is an important carrier for *I* in the ReBAMB and determines *I* mobility and fate (Santschi et al. 2017; Whitehead 1984; Xu et al. 2011b). But, due to the low DOC mobility only small amounts of DOI are mobilized.

Even if *I* is mobilized in uphill soils it is likely that *I* is retained in the soil during transport either through sorption to metal-oxides or by iodination of OM especially of aromatic carbon compounds (Fox et al. 2010; Zhang et al. 2011) and in this way does not reach the stream .

This suggests little *I* input from the soils of the catchment and is supported by low *I* increase during stormflow and generally low *I* concentrations in stream water (around $1 \mu\text{g L}^{-1}$) during base- and even quickflow conditions compared to the global *I* mean concentration in river water ranging between $0.5\text{-}20 \mu\text{g L}^{-1}$.

It can therefore be concluded that almost no *I* is mobilized in the ReBAMB and just small amounts of *I* from precipitation reach Q_M during heavy rain events due to the high *I* fixation in the soil.

4.3.1 Iodine speciation in Q_M

Since *I* speciation was not conducted, present *I* species can only be estimated.

Considering a solely inorganic aqueous system, the speciation of *I* is redox sensitive. The expected *I* species under thermodynamic considerations in Q_M (Fig. 20) would be I^- . I^- is the most mobile form of *I* because it has a low affinity for sorption on soil particles.

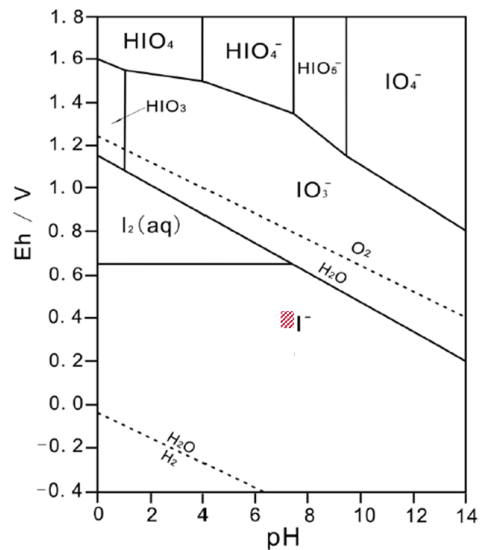


Figure 20 Eh-pH diagram for iodine species in water at 25 °C, adapted from Li et al. (2013). The type of I species expected under thermodynamic considerations in Q_M as the dominant species is shaded red.

Because of the high OM content in the soils of the ReBAMB, the most abundant I species is probably DOI (Gilfedder et al. 2010; Li et al. 2014; Santschi and Schwehr 2004; Shetaya et al. 2012; Xu et al. 2011b) formed with high molecular weight OM (Santschi and Schwehr 2004) especially humic and fulvic acids (Rädlinger and Heumann 2000; Shetaya et al. 2012; Steinberg et al. 2008a; Steinberg et al. 2008b).

4.3.2 Fate of iodine in stream

I is wiped off from river water through the formation and co-precipitation of colloidal organic-metal-complexes in sediments (Li et al. 2013; Qian et al. 2017). Especially in periods of low flow velocity or stagnation, I accumulation in bottom water and sediments is high. Thus, this leads to higher I accumulation in Q_L because flow velocity is lower than that of Q_R and Q_M . Biofilms of Q_M exhibit the lowest I concentration due to the highest flow velocity (Fig. 16). Reductive changes may lead to the release of I into the water.

4.4 Comparison between C_L and C_R

In comparison to Q_M and Q_R , Q_L had the lowest element fluxes, including I, DOC and Fe. In contrast, concentrations in stream water were almost all higher in Q_L than in Q_R , including Fe, I and DOC (Fig. 13). Exceptions are for example SO_4^{2-} , Cr, V, U, Ti and Ca. Therefore, the catchment size is the main controlling factor of element export. Further, the higher water amounts that

discharge in Q_R per second (Fig. 12) lead to the dilution of element concentrations in comparison to C_L .

Nevertheless, the soils in C_R exhibit smaller amounts of clay and greater amounts of sand, leading to more porous soils in comparison to the soils in C_L (Schulz 2018). Thus, the ability to fix I or DOC is decremented in C_R . Therefore, one could have expected that Q_R would show higher I and DOC concentrations in stream water (da Costa et al. 2017). On the other hand, more porous soils allow water to infiltrate faster and to a greater extent. Especially because the maximum slope in C_R is smaller than in C_L . In C_L , steeper slopes and lower porosity accelerate the flow velocity of water runoff and reduce the infiltration capacity of water. This in turn enhances erosive forces of surface runoff, the transport of particulate matter and of associated elements. Furthermore, the lateral flow and the percolation of infiltrating water in C_L is slower due to finer texture, resulting in a prolonged residence time of water in the soil compared to C_R . This in turn accelerates soil-water interactions and biogeochemical reactions that can mobilize elements (Dupas et al. 2017). This supports the higher element concentrations found in Q_L .

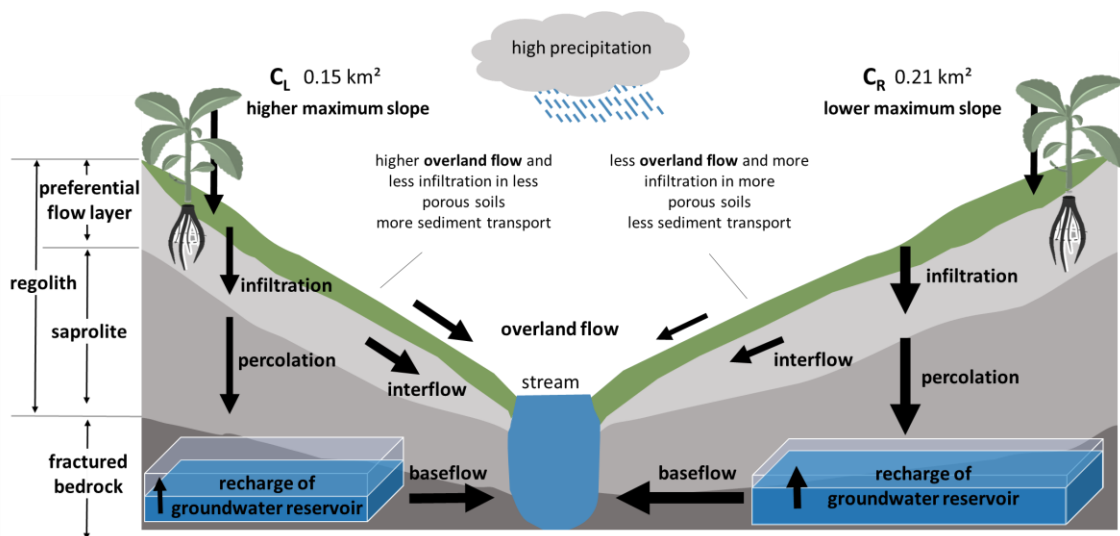


Figure 21 Schematic representation of the hydrologic processes during wet conditions at hillslope scale in the catchments of the left tributary (C_L) and the right tributary (C_R). The thickness of the arrows symbolises the relative contribution to total discharge in the respective catchment.

Activated lateral subsurface flow (and under extreme conditions overland flow) during rainfall events leads to the enrichment of most of the elements in Q_M (Fig. 10) that are also enriched in Q_L (Mn, La, Ce, Fe, DOC, Y, NO_3^- , K) compared to Q_R (Fig. 13). At the same time, elements that are depleted during rainfall events (U, V) in Q_M are depleted in Q_R in comparison to Q_L . Therefore, shallow subsurface flow paths seem to be more important in C_L than in C_R . In C_R ,

lateral subsurface flow plays a subordinate role because more rain water infiltrates and discharges as baseflow (Fig. 21).

The mean values of pH, Eh, EC and Tds were nearly identical in both tributaries, but slightly higher in Q_L (average: Q_L : $39.4 \mu\text{S} \cdot \text{cm}^{-1}$, 19.8 ppm; Q_R : $37.4 \mu\text{S} \cdot \text{cm}^{-1}$, 18.7 ppm). This supports the hypothesis that differences in flow paths are marginal between both catchments and the main difference is the size and amount of water that discharges.

4.5 Iodine chemistry compared to Br chemistry based on the I:Br-ratio

The concentration of Br in throughfall is more than 3.5 times higher than the concentration of I, indicated by a relatively small I:Br-ratio of 0.28. The I:Br ratio in solid samples is close to one (Schulz 2018). Based on the small ratio in the throughfall and the higher ratio in the soil, it seems that I exhibits a much stronger sorption and lower mobility compared to Br. This is also supported by the low I:Br-ratios in F1-leachates and in adjacent rivers.

It can be presumed that all profiles would show the same pattern in I:Br-ratios if all profiles were sampled in three depths. Leading to the assumption that the I:Br-ratio first decreases from topsoil horizons to the I accumulation horizons and is strongly increasing in deeper horizons (Fig. 17). Because in all depths the ratio is below one, Br exhibits in all depth a higher mobility or leachability than I. But in vertical consideration the difference in mobility is more pronounced in the I accumulation horizon, evidenced by the lowest I:Br-ratio compared to the horizons above and below. Meaning that Br may reach deeper into the soils. Furthermore, the I:Br-ratio of the leachates of F4 is higher than one in the entire profile, with a mean value of 2.6 indicating that I is associated with Fe-oxides to a higher extent than Br, most likely as Org-I-complexes. The complexation with OM and Fe-oxides is responsible for higher I retention in the soils in relation to Br.

Both, Br and I are biophilic elements and are concentrated in organic-rich soils (Gilfedder et al. 2011; Levy et al. 2018). The incorporation of Br into OM was found during decomposition of OM. The halogenation (Br and I) of OM can occur by abiotic or biotic processes (enzymatic reactions) (Martínez-Cortizas et al. 2016). But I exhibits a higher affinity to sorb to OM than Br. The oxidation potential of I is lower (lower electronegativity) than that of Br. Thus, I is more easily oxidized to HOI than Br to HOBr (Gilfedder et al. 2011). The oxidation can be catalysed by haloperoxidases (Li et al. 2011; Martínez-Cortizas et al. 2016). Once in the HOI/ HOBr-form, they incorporate quickly into OM via covalent bindings to C. In comparison, the I-C bond is much weaker than the Br-C bond. This in turn leads to the release of I during decomposition of OM

rather than the release of Br (Gilfedder et al. 2011). Furthermore, inorganic species of Br, bromide (Br^-), are more likely to occur in soils and aqueous system than inorganic species of I (Gilfedder et al. 2011). In precipitation and tributaries Br^- is the main Br species (Gilfedder et al. 2011). The higher input of Br as inorganic species via atmospheric deposition leads to lower organic species from the beginning of halogen input compared to I. And the higher oxidation potential leads to lower organobromine formation. As a consequence, Br is more mobile compared to I because the formation of Org-I-metal-complexes is much faster.

The higher mobility of Br compared to I is also expressed in the significant correlation between the discharge and Br concentration of Q_M ($r_s=0.61$, $p<0.05$) (Tab. 5). Especially the discharge under baseflow conditions is significantly correlated with Br ($r_s=0.73$, $p<0.01$). No correlation could be indicated for I concentrations in stream water. It seems that percolating rainwater and groundwater discharge is responsible for Br transport into the stream. Moreover, Br concentration in throughfall is lower than the concentration in stream water during baseflow and even quickflow conditions. Thus, it is likely that Br is mobilized from the soils and that soils represent a source of Br to stream waters in the ReBAMB.

5 Outlook

Further studies may provide relevant information about long term fate of incoming *I* and retention capacities in tropical soils. This could also include batch or soil column experiments to identify basic process knowledge about *I* mobility under different pH and redox conditions in tropical soils.

But also, *I* tracer studies may help to trace back atmospheric *I* inputs and may provide knowledge about the storage capacity of *I* in the ecosystem. Also, a comparison between the stable isotope ^{127}I and the radioisotope ^{129}I may help to trace *I* transport mechanisms and distribution pathways in the tropics since recent human nuclear activity has led to elevated ^{129}I concentrations and increased $^{129}\text{I}:^{127}\text{I}$ -ratio (Hou et al. 2009).

I speciation analysis would reveal important information about the degree to which *I* is bound as DOI-metal-complex or as inorganic *I* to solid phases and which species are released or accumulated.

It could be interesting to perform two different sequential extractions of the same soil sample. One that extracts first the *I* bound to reducible components with subsequent extraction of *I* bound to OM as conducted in this thesis. And the other extraction would extract the other way around to determine if the sequential extraction underestimates *I* bound to the respective subsequent extraction step. This would support the assumption that *I* is mainly sorbed as I-organic-metal-complex in the soils of the ReBAMB.

6 Conclusions

I is derived mostly from the atmosphere and is retained in the soil, since the parent materials (basalt and andesit) contain low *I* contents. *I* leachability and transport to streams is generally low. On average only 0.24 % of total *I* were water extractable and represent the mobile phase in the soil. There are two different *I* mobility patterns in the soils of the ReBAMB. In L1, R1 and R5 *I* mobility was the highest in topsoil horizons and declined with increasing depth. In L3 and R3, *I* mobility was the lowest in the accumulation horizon of *I*. It is likely that *I* is retained due to iodination of OM and formation of OM-complexes after deposition and is mobilized in small amounts as DOI during heavy rain events and as a consequence of decomposition processes. Due to the high amounts of *I* associated with metal-oxides in these soils and the presence of an *I* accumulation horizon, *I* is likely fixed and stabilized by Fe-oxides as DOM-*I*-metal-complex.

Based on the RDF-method, greatest amounts of precipitation reach the stream water as baseflow due to the high porosity of the soils, high infiltration and percolation rates (due to PFPs) and the reduction of overland flows as a result of the high tree density. Due to higher *I* concentration in throughfall compared to stream concentrations, it is likely that the soils of the catchment are not a source but rather a sink for *I*. Heavy rainfall events have only a very small influence on *I* mobilization. Groundwater discharge and to a lesser extent precipitation are the main *I* inputs to the streams in the catchment. As *I* is associated to OM and metal-oxides mutual interactions are affecting *I* mobilization. Even if *I* is mobilized in uphill soils it is likely that *I* is retained in the soil during transport either through sorption to metal-oxides or by iodination of OM. Old, weathered tropical soils, rich in OM and sesquioxides, inhibit *I* release and support strong *I* accumulation through strong sorption. Since incoming *I* is stored and not mobilized it can be concluded that the studied ecosystem is not saturated with *I* and exhibits high *I* retention capacities.

7 Acknowledgments

First of all, I thank Prof. Harald Biester for the great opportunity to carry out my master thesis in Costa Rica, his support and for supervising this work. I would like to thank Petra Schmidt and Adelina Caeian for all their support from the beginning, the planning of the project “Costa Rica” until the completion of the thesis and especially during laboratory work. I also would like to thank Katrin Schulz for our great time working together in Costa Rica and Germany. I would like to express my gratitude to Dr. Christian Birkel for his involvement in field work and support with all my hydrological and analytical questions. Further I thank the team from the Rodolfo Ortiz Biological Station for their friendly hospitality, especially “Will” for the freshly prepared meals and snacks. I would also like to thank Prof. Dr. Boris Schröder-Esselbach for accepting to be my second supervisor. I want to thank all proof readers for all their valuable comments and suggestions. Finally, even though it is unrelated to the content and quality of the thesis, I want to thank my family and friends for their support and encouragement.

8 References

- Amachi, S. (2008): Microbial contribution to global iodine cycling. Volatilization, accumulation, reduction, oxidation, and sorption of iodine. In *Microbes Environ.* 23 (4), pp. 269–276.
- Amachi, S.; Kamagata, Y.; Kanagawa, T.; Muramatsu, Y. (2001): Bacteria mediate methylation of iodine in marine and terrestrial environments. In *Appl Environ Microbiol* 67 (6), pp. 2718–2722.
- Anschutz, P.; Sundby, B.; Lefrançois, L.; Luther, G. W.; Mucci, A. (2000): Interactions between metal oxides and species of nitrogen and iodine in bioturbated marine sediments. In *Geochim. Cosmochim. Acta* 64 (16), pp. 2751–2763.
- Arnold, J. G.; Allen, P. M. (1999): Automated methods for estimating baseflow and ground water recharge from streamflow records. In *J Am Water Resources Assoc* 35 (2), pp. 411–424.
- Ashworth, D. J. (2009): Transfers of Iodine in the Soil–Plant–Air System. Solid–Liquid Partitioning, Migration, Plant Uptake and Volatilization. In Gerard N. Burrow, Ronald Ross Watson, Victor R. Preedy (Eds.): *Comprehensive handbook of iodine. Nutritional, biochemical, pathological, and therapeutic aspects.* Amsterdam, Boston: Elsevier Academic Press/Elsevier, pp. 107–118.
- Benoist, B. de (2004): Iodine status worldwide. WHO global database on iodine deficiency. Geneva: Dept. of Nutrition for Health and Development, World Health Organization.
- Benoist, B. de; McLean, E.; Andersson, M.; Rogers, L. (2008): Iodine deficiency in 2007: global progress since 2003. In *Food Nutr Bull* 29 (3), pp. 195–202.
- Biester, H.; Keppler, F.; Putschew, A.; Martinez-Cortizas, A.; Petri, M. (2004): Halogen Retention, Organohalogenes, and the Role of Organic Matter Decomposition on Halogen Enrichment in Two Chilean Peat Bogs. In *Environ. Sci. Technol.* 38 (7), pp. 1984–1991.
- Birkel, C. (2017): personal communication.
- Boucher, J. L.; Carey, S. K. (2010): Exploring runoff processes using chemical, isotopic and hydrometric data in a discontinuous permafrost catchment. In *Hydrol Res* 41 (6), p. 508.
- Bowley, H. E.; Young, S. D.; Ander, E. L.; Crout, N. M. J.; Watts, M. J.; Bailey, E. H. (2016): Iodine binding to humic acid. In *Chemosphere* 157, pp. 208–214.
- Broder, T.; Biester, H. (2017): Linking major and trace element concentrations in a headwater stream to DOC release and hydrologic conditions in a bog and peaty riparian zone. In *Appl Geochem* 87, pp. 188–201.

- Calderon, H.; Uhlenbrook, S. (2016): Characterizing the climatic water balance dynamics and different runoff components in a poorly gauged tropical forested catchment, Nicaragua. In *Hydrolog Sci J* 61 (14), pp. 2465–2480.
- Cheng, Y.; Ogden, F. L.; Zhu, J. (2017): Earthworms and tree roots. A model study of the effect of preferential flow paths on runoff generation and groundwater recharge in steep, saprolitic, tropical lowland catchments. In *Water Resour. Res.* 53 (7), pp. 5400–5419.
- Correa, A.; Windhorst, D.; Tetzlaff, D.; Crespo, P.; Célleri, R.; Feyen, J.; Breuer, L. (2017): Temporal dynamics in dominant runoff sources and flow paths in the Andean Páramo. In *Water Resour. Res.* 53 (7), pp. 5998–6017.
- Couture, R. A.; Seitz, M. G. (1983): Sorption of anions of iodine by iron oxides and kaolinite. In *Waste Manag* 4 (4), pp. 301–306.
- Crespo, P. J.; Feyen, J.; Buytaert, W.; Bücker, A.; Breuer, L.; Frede, H.-G.; Ramírez, M. (2011): Identifying controls of the rainfall–runoff response of small catchments in the tropical Andes (Ecuador). In *J Hydrol (Amst)* 407 (1-4), pp. 164–174.
- da Costa, E. N. D.; Souza, J. C. de; Pereira, M. A.; Souza, M. F. L. de; Souza, W. F. L. de; da Silva, D. M. L. (2017): Influence of hydrological pathways on dissolved organic carbon fluxes in tropical streams. In *Ecol Evol* 7 (1), pp. 228–239.
- Dai, J. L.; Zhang, M.; Hu, Q. H.; Huang, Y. Z.; Wang, R. Q.; Zhu, Y. G. (2009): Adsorption and desorption of iodine by various Chinese soils. II. Iodide and iodate. In *Geoderma* 153 (1-2), pp. 130–135.
- Deb, S. K.; Shukla, M. K. (2011): A Review of Dissolved Organic Matter Transport Processes Affecting Soil and Environmental Quality. In *J Environment Analytic Toxicol* 01 (02).
- Dissanayake, C.B.; Chandrajith, R. (1999): Medical geochemistry of tropical environments. In *Earth Sci Rev* 47 (3-4), pp. 219–258.
- Duchaufour, P. (Ed.) (1982): *Pedology*. Dordrecht: Springer Netherlands.
- Dupas, R.; Musolff, A.; Jawitz, J. W.; Rao, P. S. C.; Jäger, C. G.; Fleckenstein, J. H.; Rode, M.; Borchardt, D. (2017): Carbon and nutrient export regimes from headwater catchments to downstream reaches. In *Biogeosciences* 14 (18), pp. 4391–4407.
- Elsenbeer, H.; Lack, A.; Cassel, K. (1995): Chemical fingerprints of hydrological compartments and flow paths at La Cuenca, Western Amazonia. In *Water Resour. Res.* 31 (12), pp. 3051–3058.

References

- Farrick, K. K.; Branfireun, B. A. (2015): Flowpaths, source water contributions and water residence times in a Mexican tropical dry forest catchment. In *J Hydrol (Amst)* 529, pp. 854–865.
- Fox, P. M.; Kent, D. B.; Davis, J. A. (2010): Redox transformations and transport of cesium and iodine (-1, 0, +5) in oxidizing and reducing zones of a sand and gravel aquifer. In *Environ. Sci. Technol.* 44 (6), pp. 1940–1946.
- Fuge, R.; Johnson, C. C. (1986): The geochemistry of iodine - a review. In *Environ Geochem Health* 8 (2), pp. 31–54.
- Gilfedder, B. S.; Lai, S.; Petri, M.; Biester, H.; Hoffmann, T. (2008): Iodine speciation in rain, snow and aerosols and possible transfer of organically bound iodine species from aerosol to droplet phases. In *Atmos Chem Phys Discuss* 8 (2), pp. 7977–8008.
- Gilfedder, B. S.; Petri, M.; Wessels, M.; Biester, H. (2010): An iodine mass-balance for Lake Constance, Germany. Insights into iodine speciation changes and fluxes. In *Geochim. Cosmochim. Acta* 74 (11), pp. 3090–3111.
- Gilfedder, B. S.; Petri, M.; Wessels, M.; Biester, H. (2011): Bromine species fluxes from Lake Constance's catchment, and a preliminary lake mass balance. In *Geochim. Cosmochim. Acta* 75 (12), pp. 3385–3401.
- Grimvall, A.; Laniewski, K.; Borén, H.; Jonsson, S.; Kaugare, S. (1994): Organohalogenes of natural or unknown origin in surface water and precipitation. In *Toxicol Environ Chem* 46 (3), pp. 183–196.
- Gutchess, K. M.; Garvin, S.; Jin, L.; Lu, W.; Levy, Z.; Lautz, L. K.; Lu, Z. (2017): Evaluating the Natural Transport Pathways of Iodine in Headwater Catchments. In. Northeast/North-Central Geological Society of America Joint Section Meeting- 2017, 19-21 March 2017: Geological Society of America (Geological Society of America Abstracts with Programs).
- Guzmán, P.; Batelaan, O.; Huysmans, M.; Wyseure, G. (2015): Comparative analysis of baseflow characteristics of two Andean catchments, Ecuador. In *Hydrol. Process.* 29 (14), pp. 3051–3064.
- Hessen, D. O.; Andersen, T.; Tominaga, K.; Finstad, A. G. (2017): When soft waters becomes softer; drivers of critically low levels of Ca in Norwegian lakes. In *Limnol. Oceanogr.* 62 (1), pp. 289–298.
- Hope, D.; Billett, M. F.; Cresser, M. S. (1994): A review of the export of carbon in river water. Fluxes and processes. In *Environ. Pollut* 84 (3), pp. 301–324.

- Hou, X.; Hansen, V.; Aldahan, A.; Possnert, G.; Lind, O. C.; Lujaniene, G. (2009): A review on speciation of iodine-129 in the environmental and biological samples. In *Anal Chim Acta* 632 (2), pp. 181–196.
- Hou, X.L.; Fogh, C.L.; Kucera, J.; Andersson, K.G.; Dahlgard, H.; Nielsen, S.P. (2003): Iodine-129 and Caesium-137 in Chernobyl contaminated soil and their chemical fractionation. In *Sci. Total Environ.* 308 (1-3), pp. 97–109.
- Hu, Q.; Moran, J. E.; Blackwood, V. (2009): Geochemical Cycling of Iodine Species in Soils. In : *Comprehensive Handbook of Iodine*: Elsevier, pp. 93–105.
- Hu, Q.; Zhao, P.; Moran, J. E.; Seaman, J. C. (2005): Sorption and transport of iodine species in sediments from the Savannah River and Hanford Sites. In *J Contam Hydrol* 78 (3), pp. 185–205.
- Hu, Q. H.; Moran, J. E.; Gan, J. Y. (2012): Sorption, degradation, and transport of methyl iodide and other iodine species in geologic media. In *Appl Geochem* 27 (3), pp. 774–781.
- IUSS Working Group (2014): World reference base for soil resources 2014. International soil classification system for naming soils and creating legends for soil maps. Rome: FAO (World soil resources reports, 106).
- Johnson, C. C. (2003): The geochemistry of iodine and its application to environmental strategies for reducing the risks from iodine deficiency disorders. In *Brit Geol Surv* (DFID kar project R7411, Report CR/03/057N), 54pp.
- Kaiser, K.; Guggenberger, G. (2000): The role of DOM sorption to mineral surfaces in the preservation of organic matter in soils. In *Org Geochem* 31 (7-8), pp. 711–725.
- Kaplan, D. I. (2003): Influence of surface charge of an Fe-oxide and an organic matter dominated soil on iodide and pertechnetate sorption. In *Radiochim Acta* 91 (3), p. 75.
- Kaplan, D. I.; Seme, R. J. and Piepkho, M. G. (1995): Geochemical factors affecting radionuclide transport through near and far fields at a Low-Level Waste Disposal Site.
- Koch-Steindl, H.; Pröhl, G. (2001): Considerations on the behaviour of long-lived radionuclides in the soil. In *Radiat Environ Biophys* 40 (2), pp. 93–104.
- Kodama, S.; Takahashi, Y.; Okumura, K.; Uruga, T. (2006): Speciation of iodine in solid environmental samples by iodine K-edge XANES. Application to soils and ferromanganese oxides. In *Sci. Total Environ.* 363 (1-3), pp. 275–284.
- Leri, A. C.; Myneni, S. C.B. (2012): Natural organobromine in terrestrial ecosystems. In *Geochim. Cosmochim. Acta* 77, pp. 1–10.

References

- Levy, Z. F.; Mills, C. T.; Lu, Z.; Goldhaber, M. B.; Rosenberry, D. O.; Mushet, D. M.; Lautz, L. K.; Zhou, X.; Siegel, D. I. (2018): Using halogens (Cl, Br, I) to understand the hydrogeochemical evolution of drought-derived saline porewater beneath a prairie wetland. In *Chem Geol* 476, pp. 191–207.
- Li, H.-P.; Brinkmeyer, R.; Jones, W. L.; Zhang, S.; Xu, C.; Schwehr, K. A.; Santschi, P. H.; Kaplan, D. I.; Yeager, C. M. (2011): Iodide accumulation by aerobic bacteria isolated from subsurface sediments of a ¹²⁹I-contaminated aquifer at the Savannah River site, South Carolina. In *Appl Environ Microbiol* 77 (6), pp. 2153–2160.
- Li, J.; Wang, Y.; Guo, W.; Xie, X.; Zhang, L.; Liu, Y.; Kong, S. (2014): Iodine mobilization in groundwater system at Datong basin, China. Evidence from hydrochemistry and fluorescence characteristics. In *Sci. Total Environ.* 468-469, pp. 738–745.
- Li, J.; Wang, Y.; Xie, X.; Zhang, L.; Guo, W. (2013): Hydrogeochemistry of high iodine groundwater. A case study at the Datong Basin, northern China. In *Environ Sci Process Impacts* 15 (4), pp. 848–859.
- Martínez-Cortizas, A. M.; Vázquez, C. F.; Kaal, J.; Biester, H.; Casais, M. C.; Rodríguez, T. T.; Lado, L. R. (2016): Bromine accumulation in acidic black colluvial soils. In *Geochim. Cosmochim. Acta* 174, pp. 143–155.
- Moore, T. R. (1989): Dynamics of dissolved organic carbon in forested and disturbed catchments, Westland, New Zealand. 1. Maimai. In *Water Resour. Res.* 25 (6), pp. 1321–1330.
- Moreda-Piñeiro, A.; Romarís-Hortas, V.; Bermejo-Barrera, P. (2011): A review on iodine speciation for environmental, biological and nutrition fields. In *J. Anal. At. Spectrom.* 26 (11), p. 2107.
- Muramatsu, Y.; Yoshida, S.; Fehn, U.; Amachi, S.; Ohmomo, Y. (2004): Studies with natural and anthropogenic iodine isotopes. Iodine distribution and cycling in the global environment. In *J Environ Radioact* 74 (1-3), pp. 221–232.
- Nathan, R. J.; McMahon, T. A. (1990): Evaluation of automated techniques for base flow and recession analyses. In *Water Resour. Res.* 26 (7), pp. 1465–1473.
- Otosaka, S.; Schwehr, K. A.; Kaplan, D. I.; Roberts, K. A.; Zhang, S.; Xu, C.; Li, H.-P.; Ho, Y.-F.; Brinkmeyer, R.; Yeager, C. M.; Santschi, P. H. (2011): Factors controlling mobility of ¹²⁷I and ¹²⁹I species in an acidic groundwater plume at the Savannah River Site. In *Sci. Total Environ.* 409 (19), pp. 3857–3865.

- Pearce, A. J.; Stewart, M. K.; Sklash, M. G. (1986): Storm Runoff Generation in Humid Headwater Catchments. 1. Where Does the Water Come From? In *Water Resour. Res.* 22 (8), pp. 1263–1272.
- Qian, K.; Li, J.; Xie, X.; Yang, Y. (2017): Effects of Organic and Inorganic Colloids on Iodine Mobilization in Groundwater of the Datong Basin, Northern China. In *Procedia Earth Planet. Sci.* 17, pp. 153–156.
- Rädlinger, G.; Heumann, K. G. (2000): Transformation of Iodide in Natural and Wastewater Systems by Fixation on Humic Substances. In *Environ. Sci. Technol.* 34 (18), pp. 3932–3936.
- Renshaw, J. C.; Handley-Sidhu, S.; Brookshaw, D. R. (2011): Chapter 7. Pathways of Radioactive Substances in the Environment. In R. M. Harrison, R. E. Hester (Eds.): *Nuclear Power and the Environment*. Cambridge: Royal Society of Chemistry (Issues in Environmental Science and Technology), pp. 152–176.
- Santschi, P. H.; Schwehr, K. A. (2004): $^{129}\text{I}/(^{127}\text{I})$ as a new environmental tracer or geochronometer for biogeochemical or hydrodynamic processes in the hydrosphere and geosphere. The central role of organo-iodine. In *Sci. Total Environ.* 321 (1-3), pp. 257–271.
- Santschi, P. H.; Xu, C.; Zhang, S.; Schwehr, K. A.; Grandbois, R.; Kaplan, D. I.; Yeager, C. M. (2017): Iodine and plutonium association with natural organic matter. A review of recent advances. In *Appl Geochem* 85, pp. 121–127.
- Schellekens, J.; Scatena, F. N.; Bruijnzeel, L. A.; van Dijk, A. I. J. M.; Groen, M. M. A.; van Hogeand, R. J. P. (2004): Stormflow generation in a small rainforest catchment in the Luquillo Experimental Forest, Puerto Rico. In *Hydrol. Process.* 18 (3), pp. 505–530.
- Schmitz, K.; Aumann, D. C. (1995): A study on the association of two iodine isotopes, of natural ^{127}I and of the fission product ^{129}I , with soil components using a sequential extraction procedure. In *J Radioanal Nucl Chem* 198 (1), pp. 229–236.
- Scholl, M. A.; Shanley, J. B.; Murphy, S. F.; Willenbring, J. K.; Occhi, M.; González, G. (2015): Stable-isotope and solute-chemistry approaches to flow characterization in a forested tropical watershed, Luquillo Mountains, Puerto Rico. In *Appl Geochem* 63, pp. 484–497.
- Schulz, K. (2018): Iodine distribution, speciation and mobility in volcanic soils of a tropical forest. – a case study from Costa Rica. Master thesis. Braunschweig: Technical University of Braunschweig.
- Schwehr, K. A.; Santschi, P. H.; Kaplan, D. I.; Yeager, C. M.; Brinkmeyer, R. (2009): Organo-Iodine Formation in Soils and Aquifer Sediments at Ambient Concentrations. In *Environ. Sci. Technol.* 43 (19), pp. 7258–7264.

References

- Sheppard, M. I.; Hawkins, J. L.; Smith, P. A. (1996): Linearity of Iodine Sorption and Sorption Capacities for Seven Soils. In *J. Environ. Qual.* 25 (6), p. 1261.
- Sheppard, M. I.; Thibault, D. H.; McMurry, J.; Smith, P. A. (1995): Factors affecting the soil sorption of iodine. In *Water Air Soil Pollut* 83 (1-2), pp. 51–67.
- Shetaya, W. H.; Young, S. D.; Watts, M. J.; Ander, E. L.; Bailey, E. H. (2012): Iodine dynamics in soils. In *Geochim. Cosmochim. Acta* 77, pp. 457–473.
- Shimamoto, Y. S.; Itai, T.; Takahashi, Y. (2010): Soil column experiments for iodate and iodide using K-edge XANES and HPLC–ICP-MS. In *J Geochem Explor* 107 (2), pp. 117–123.
- Shimamoto, Y. S.; Takahashi, Y.; Terada, Y. (2011): Formation of organic iodine supplied as iodide in a soil-water system in Chiba, Japan. In *Environ. Sci. Technol.* 45 (6), pp. 2086–2092.
- Sklash, M. G.; Stewart, M. K.; Pearce, A. J. (1986): Storm Runoff Generation in Humid Headwater Catchments. 2. A Case Study of Hillslope and Low-Order Stream Response. In *Water Resour. Res.* 22 (8), pp. 1273–1282.
- Smoleń, S.; Ledwozyw-Smoleń, I.; Sady, W. (2016): The role of exogenous humic and fulvic acids in iodine biofortification in spinach (*Spinacia oleracea* L.). In *Plant Soil* 402 (1-2), pp. 129–143.
- Smyth, D.; Johnson, C. C. (2011): Distribution of iodine in soils of Northern Ireland. In *Geochem Explor Env A* 11 (1), pp. 25–39.
- Söderlund, M.; Lusa, M.; Lehto, J.; Hakanen, M. and Vaaramaa, K. (2011): Sorption of iodine, chlorine, technetium and cesium in soil. Oulkuoto: Posiva Oy (Working report, 2011-04).
- Sommer, M.; Kaczorek, D.; Kuzyakov, Y.; Breuer, J. (2006): Silicon pools and fluxes in soils and landscapes—a review. In *J. Plant Nutr. Soil Sci.* 169 (3), pp. 310–329.
- Steinberg, S. M.; Kimble, G. M.; Schmett, G. T.; Emerson, D. W.; Turner, M. F.; Rudin, M. (2008a): Abiotic reaction of iodate with sphagnum peat and other natural organic matter. In *J Radioanal Nucl Chem* 277 (1), pp. 185–191.
- Steinberg, S. M.; Schmett, G. T.; Kimble, G.; Emerson, D. W.; Turner, M. F.; Rudin, M. (2008b): Immobilization of fission iodine by reaction with insoluble natural organic matter. In *J Radioanal Nucl Chem* 277 (1), pp. 175–183.
- Stewart, M.; Cimino, J.; Ross, M. (2007): Calibration of base flow separation methods with streamflow conductivity. In *Ground Water* 45 (1), pp. 17–27.

- Trotter, W. R. (1960): The association of deafness with thyroid dysfunction. In *Br Med Bull* 16, pp. 92–98.
- Tubana, B. S.; Babu, T.; Datnoff, L. E. (2016): A Review of Silicon in Soils and Plants and Its Role in US Agriculture. In *Soil Science*, p. 1.
- Waterloo, M. J.; Oliveira, S. M.; Drucker, D. P.; Nobre, A. D.; Cuartas, L. A.; Hodnett, M. G.; Langedijk, I.; Jans, W. W. P.; Tomasella, J.; Araújo, A. C. de; Pimentel, T. P.; Múnera Estrada, J. C. (2006): Export of organic carbon in run-off from an Amazonian rainforest blackwater catchment. In *Hydrol. Process.* 20 (12), pp. 2581–2597.
- Welderufael, W. A.; Woyessa, Y. E. (2010): Stream flow analysis and comparison of base flow separation methods. Case study of the Modder River Basin in Central South Africa. In *European Water* (31), pp. 3–12.
- Whitehead, D. C. (1973): The sorption of iodide by soils as influenced by equilibrium conditions and soil properties. In *J. Sci. Food Agric.* 24 (5), pp. 547–556.
- Whitehead, D. C. (1974): The sorption of iodide by soil components. In *J. Sci. Food Agric.* 25 (1), pp. 73–79.
- Whitehead, D. C. (1978): Iodine in soil profiles in relation to iron and aluminium oxides and organic matter. In *J Soil Sci* 29 (1), pp. 88–94.
- Whitehead, D. C. (1984): The distribution and transformations of iodine in the environment. In *Environ Int* 10 (4), pp. 321–339.
- World Meteorological Organization (2008): Guide to meteorological instruments and methods of observation. 7th ed. Geneva: World Meteorological Organization (World Meteorological Organization, WMO-No. 8).
- Xu, C.; Kaplan, D. I.; Zhang, S.; Athon, M.; Ho, Y.-F.; Li, H.-P.; Yeager, C. M.; Schwehr, K. A.; Grandbois, R.; Wellman, D.; Santschi, P. H. (2015): Radioiodine sorption/desorption and speciation transformation by subsurface sediments from the Hanford Site. In *J Environ Radioact* 139, pp. 43–55.
- Xu, C.; Miller, E. J.; Zhang, S.; Li, H.-P.; Ho, Y.-F.; Schwehr, K. A.; Kaplan, D. I.; Otsuka, S.; Roberts, K. A.; Brinkmeyer, R.; Yeager, C. M.; Santschi, P. H. (2011a): Sequestration and remobilization of radioiodine (¹²⁹I) by soil organic matter and possible consequences of the remedial action at Savannah River Site. In *Environ. Sci. Technol.* 45 (23), pp. 9975–9983.

References

- Xu, C.; Zhang, S.; Ho, Y.-F.; Miller, E. J.; Roberts, K. A.; Li, H.-P.; Schwehr, K. A.; Otosaka, S.; Kaplan, D. I.; Brinkmeyer, R.; Yeager, C. M.; Santschi, P. H. (2011b): Is soil natural organic matter a sink or source for mobile radioiodine (¹²⁹I) at the Savannah River Site? In *Geochim. Cosmochim. Acta* 75 (19), pp. 5716–5735.
- Yeager, C. M.; Amachi, S.; Grandbois, R.; Kaplan, D. I.; Xu, C.; Schwehr, K. A.; Santschi, P. H. (2017): Microbial Transformation of Iodine. From Radioisotopes to Iodine Deficiency. In *Adv Appl Microbiol* 101, pp. 83–136.
- Yoshida, S.; Muramatsu, Y.; Uchida, S. (1992): Studies on the sorption of I⁻ (iodide) and IO₃⁻ (iodate) onto Andosols. In *Water Air Soil Pollut* 63 (3-4), pp. 321–329.
- Yuita, K.; Kihou, N.; Yabusaki, S.; Takahashi, Y.; Saitoh, T.; Tsumura, A.; Ichihashi, H. (2005): Behavior of Iodine in a Forest Plot, an Upland Field and a Paddy Field in the Upland Area of Tsukuba, Japan. Iodine Concentration in Precipitation, Irrigation Water, Ponding Water and Soil Water to a Depth of 2.5 m. In *Soil Sci. Plant Nutr.* 51 (7), pp. 1011–1021.
- Yuita, K.; Tanaka, T.; Abe, C.; Aso, S. (1991): Dynamics of iodine, bromine, and chlorine in soil. In *Soil Sci. Plant Nutr.* 37 (1), pp. 61–73.
- Zambrano-Bigiarini, M.; Nauditt, A.; Birkel, C.; Verbist, K.; Ribbe, L. (2017): Temporal and spatial evaluation of satellite-based rainfall estimates across the complex topographical and climatic gradients of Chile. In *Hydrol. Earth Syst. Sci.* 21 (2), pp. 1295–1320.
- Zech, W.; Schad, P. and Hintermaier-Erhard, G. (2014): Böden der Welt. Ein Bildatlas. 2. Auflage. Berlin, Heidelberg: Springer Spektrum (SpringerLink Bücher).
- Zhang, S.; Du, J.; Xu, C.; Schwehr, K. A.; Ho, Y.-F.; Li, H.-P.; Roberts, K. A.; Kaplan, D. I.; Brinkmeyer, R.; Yeager, C. M.; Chang, H.-S.; Santschi, P. H. (2011): Concentration-dependent mobility, retardation, and speciation of iodine in surface sediment from the Savannah River Site. In *Environ. Sci. Technol.* 45 (13), pp. 5543–5549.
- Zimmer, M. A.; McGlynn, B. L. (2017): Ephemeral and intermittent runoff generation processes in a low relief, highly weathered catchment. In *Water Resour. Res.* 53 (8), pp. 7055–7077.

9 Appendix

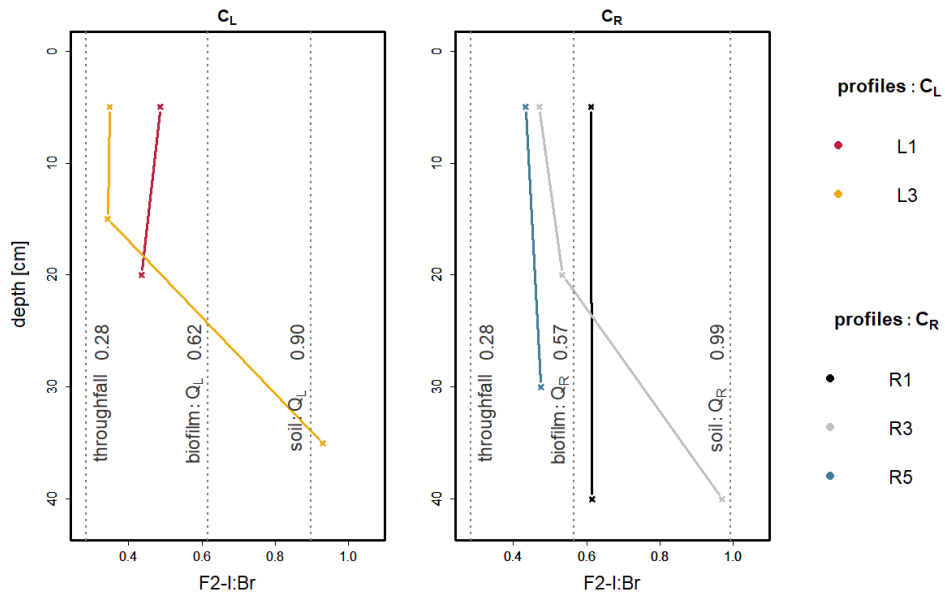


Figure 22 Extractable iodine concentrations [mg kg^{-1}] divided by extractable bromine concentration of F2 in profiles L1 (red), L3 (dark yellow), R1 (black), R3 (grey), R5 (blue). Iodine-bromine-ratios in the respective stream water, biofilm, solid soil samples (measured by Schulz (2018)) and throughfall were shown as black dashed vertical lines.

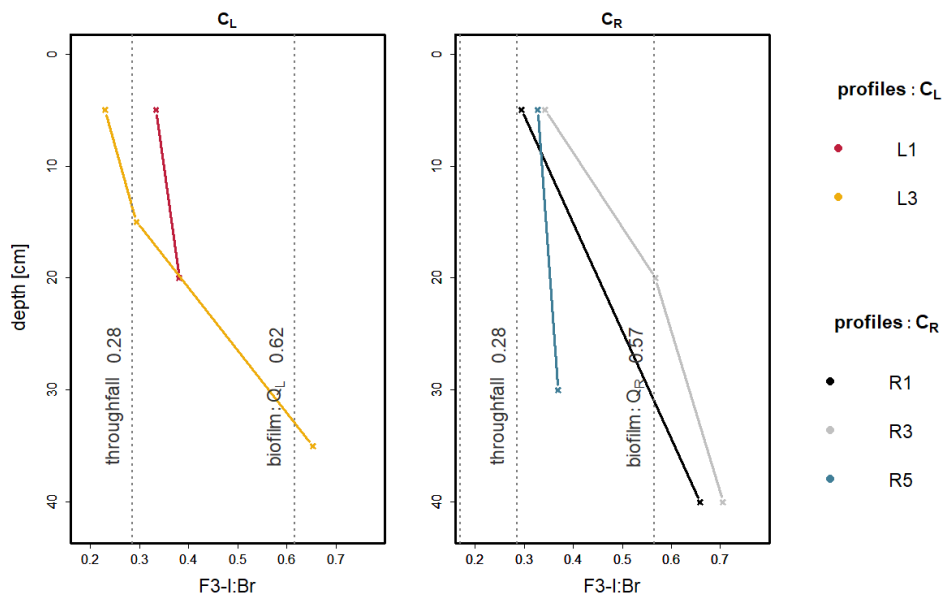


Figure 23 Extractable iodine concentrations [mg kg^{-1}] divided by extractable bromine concentration of F3 in profiles L1 (red), L3 (dark yellow), R1 (black), R3 (grey), R5 (blue). Iodine-bromine-ratios in the respective stream water, biofilm, solid soil samples (measured by Schulz (2018)) and throughfall were shown as black dashed vertical lines.

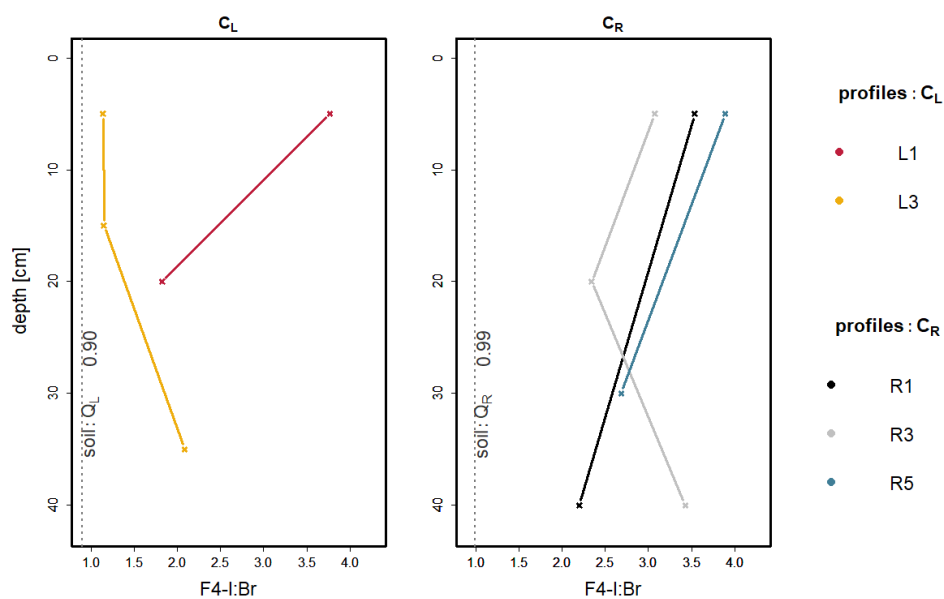


Figure 24 Extractable iodine concentrations [mg kg^{-1}] divided by extractable bromine concentration of F4 in profiles L1 (red), L3 (dark yellow), R1 (black), R3 (grey), R5 (blue). Iodine-bromine-ratios in the respective stream water, biofilm, solid soil samples (measured by Schulz (2018)) and throughfall were shown as black dashed vertical lines.

Table 8 Reference materials for solid soil analyses with certified values (CV) and measured values (MV)

Technique	Reference	No.	Element	Unit	CV	MV
Thermal extr. & ICP-MS	China Sediment	NCS DC 73312	I	mg kg^{-1}	2.9 ± 0.4	3.2
			Br	mg kg^{-1}	3.0 ± 0.6	2.4
	China Soil	DC73030	I	mg kg^{-1}	9.4 ± 1.1	4.3
XRF	LKSD4		Br	mg kg^{-1}	4.0 ± 0.7	2.6
			Fe	g kg^{-1}	28.68 ± 2	28.00
			S	g kg^{-1}	9.9 ± 0.9	5.9
			Si	g kg^{-1}	194.4 ± 3	159.2
			K	g kg^{-1}	3.4 ± 0.2	4.8
			Ca	g kg^{-1}	13 ± 1	12.7
			Zr	mg kg^{-1}	105 ± 17	85.5
			Zn	mg kg^{-1}	194 ± 19	179.2
	Y	mg kg^{-1}	23 ± 10	21.35		

Table 9 Reference materials for liquid sample analyses with certified values (CV) and measured values (MV) for stream water (MV)

Technique	Reference	No.	Element	Unit	CV	MV
ICP-MS	Roth	-	I	$\mu\text{g L}^{-1}$	5	5.4
			Br	$\mu\text{g L}^{-1}$	5	5.5
	Fluka	54704	I	$\mu\text{g L}^{-1}$	10	10.2
			Br	$\mu\text{g L}^{-1}$	10	10.8
	River Thames	LGC6019	Cr	$\mu\text{g L}^{-1}$	0.78 ± 0.2	0.73
			Fe	$\mu\text{g L}^{-1}$	287 ± 7	288.39
			Cu	$\mu\text{g L}^{-1}$	15.4 ± 1.5	14.76
			Cd	$\mu\text{g L}^{-1}$	0.11 ± 0.02	0.16
			Pb	$\mu\text{g L}^{-1}$	5.2 ± 0.3	4.62
	SPS-SW1	-	B	$\mu\text{g L}^{-1}$	50 ^b	48.04
			Sc	$\mu\text{g L}^{-1}$	0.50 ± 0.01	0.53
			V	$\mu\text{g L}^{-1}$	10.0 ± 0.1	9.96
			Cr	$\mu\text{g L}^{-1}$	2.0 ± 0.02	1.97
			Fe	$\mu\text{g L}^{-1}$	20 ± 1	19.84
			Mn	$\mu\text{g L}^{-1}$	10.0 ± 0.1	9.89
			Co	$\mu\text{g L}^{-1}$	2.0 ± 0.02	1.97
			Cu	$\mu\text{g L}^{-1}$	20 ± 1	19.31
			Ni	$\mu\text{g L}^{-1}$	10.0 ± 0.1	9.60
			As	$\mu\text{g L}^{-1}$	10.0 ± 0.1	10.15
			Se	$\mu\text{g L}^{-1}$	2.0 ± 0.02	2.43
			Rb	$\mu\text{g L}^{-1}$	10.0 ± 0.1	9.77
			Sr	$\mu\text{g L}^{-1}$	50.0 ± 0.5	51.67
			Y	$\mu\text{g L}^{-1}$	0.50 ± 0.01	0.05
			Mo	$\mu\text{g L}^{-1}$	10.0 ± 0.1	10.33
	Cd	$\mu\text{g L}^{-1}$	0.50 ± 0.01	0.55		
	Ba	$\mu\text{g L}^{-1}$	50 ± 1	47.46		
La	$\mu\text{g L}^{-1}$	0.50 ± 0.01	0.43			
Ce	$\mu\text{g L}^{-1}$	0.50 ± 0.01	0.47			
Tl		0.50 ± 0.01	0.60			
Pb	$\mu\text{g L}^{-1}$	5.0 ± 0.1	4.79			
U	$\mu\text{g L}^{-1}$	0.50 ± 0.01	0.37			
ICP-AES	River Thames	LGC6019	Ca	mg L^{-1}	109 ± 3	107.5
			K	mg L^{-1}	4.78 ± 0.12	4.72
			Mg	mg L^{-1}	4.62 ± 0.12	4.6
			Na	mg L^{-1}	24.7 ± 0.5	25.7
			Zn	$\mu\text{g L}^{-1}$	59.7 ± 2.5	60.3
IC	Roth	A19960	Cl^-	mg L^{-1}	10.04 ± 0.039	10.74
			NO_3^-	mg L^{-1}	25.247 ± 0.103	23.79
			SO_4^{2-}	mg L^{-1}	30.175 ± 0.11	26.42
	Sigma-Aldrich	QC1364	Cl^-	mg L^{-1}	123 ± 2.20	123.15
			NO_3^-	mg L^{-1}	34.2 ± 0.609	34.36
			SO_4^{2-}	mg L^{-1}	78.1 ± 1.39	78.45
TOC	TOC20		DOC	mg L^{-1}	20	21.67 ± 0.3
	Mauri	09	DOC	mg L^{-1}	5.92 ± 0.77	6.82 ± 0.31

Table 10 Reference materials for liquid sample analyses with certified values (CV) and measured values (MV) for leachates (F1-F5)

Technique	Reference	No.	Element	Unit	CV	F1 MV	F2 MV	F3 MV	F4 MV
ICP-MS	Roth	-	I	$\mu\text{g L}^{-1}$	5	5.3	5.5	4.4	5.6
	Fluka	54704	I	$\mu\text{g L}^{-1}$	10	9.6	9.6	8.1	8.3
	Roth	-	Br	$\mu\text{g L}^{-1}$	5	5.8	4.9	4.8	5.5
	Fluka	54704	Br	$\mu\text{g L}^{-1}$	10	10.5	9.9	9.4	9.3